Atmospheric Sounding by TAMDAR over Keflavík Airport, Iceland – Comparison with Traditional Atmospheric Sounding Methods

Arnór Tumi Jóhannsson

Veðurstofa
Íslands

Atmospheric Sounding by TAMDAR over Keflavík Airport, Iceland – Comparison with Traditional Atmospheric Sounding Methods

Arnór Tumi Jóhannsson, Veðurstofa Íslands

Lykilsíða

Veðurstofa
Íslands

Skýrsla nr. VÍ 2017-002	Dags. Mars 2017	ISSN: 1670-8261	Opin ☒ Lokuð ☐ Skilmálar:

Heiti skýrslu / Aðal- og undirtitill: Atmospheric Sounding by TAMDAR over Keflavík Airport, Iceland – Comparison with Traditional Atmospheric Sounding Methods	Upplag: 8 Fjöldi síðna: 70
	Framkvæmdastjóri sviðs: Jórunn Harðardóttir
Höfundar: Arnór Tumi Jóhannsson	Verkefnisstjóri: Guðrún Nína Petersen
	Verknúmer: 3507-0-0007
Gerð skýrslu/verkstig:	Málsnúmer: 2017-94

Unnið fyrir:

Samvinnuaðilar:

Útdráttur:

Verkefni þetta var unnið sem lokaverkefni í grunnámi í jarðeðlisfræði við Háskóla Íslands. Háloftamælingar með veðurkanna (e. radiosonde) voru bornar saman við háloftamælingar framkvæmdar af TAMDAR yfir Keflavíkurflugvelli. Tilgangur verkefnisins var að meta mögulegan ávinning þess að innleiða TAMDAR-gögn í athugunar- og spákerfi Veðurstofu Íslands. Þrátt fyrir fremur lítið gagnasafn og mikinn breytileika í rúmi var ályktað sem svo, að hitamælingar TAMDAR væru áreiðanlegar og í góðu samræmi við hitamælingar veðurkanna. Niðurstöður verkefnisins benda til þess að vindáttarmælingar TAMDAR séu almennt góðar. TAMDAR nemur breytingar í loftraka og eru loftrakamælingar í samræmi við spár að allnokkru leyti. Gæði vindhraðamælinga TAMDAR eru torræð, en yfirleitt má skýra ósamræmi milli vindhraðamælinga veðurkanna og TAMDAR með þeim breytileika sem fram kemur í spám eða athugunum. Innleiðing TAMDAR-gagna yrði líkast til ágætis viðbót við þau gögn sem löngum hafa legið til grundvallar háloftaathugunum á Íslandi; slík viðbót yki víðfeðmi og tíðni háloftamælinga yfir Íslandi.

Lykilorð: Háloftaathuganir, flugveður, flugveðurspá, atmospheric profiling, atmospheric sounding, radiosonde, weather balloon, weather forecast, aviation meteorology, aviation weather, TAMDAR	Undirskrift framkvæmdastjóra sviðs: Undirskrift verkefnisstjóra: GN PETERSEN Yfirfarið af:

Abstract

Tropospheric measurements by radiosonde and Tropospheric Airborne Meteorological Data Reporting (TAMDAR) over Keflavík airport, Iceland, were compared in an effort to assess the potential benefit of implementing TAMDAR data in the observations and forecasting system of the Icelandic Meteorological Office (IMO). Despite a relatively small dataset and considerable spatial variability in the data, it was concluded that TAMDAR performs well in measuring temperature. Temperature measurements of radiosonde and TAMDAR were generally in good agreement. Furthermore, the results suggest that TAMDAR does well at assessing wind direction. TAMDAR detects variations in relative humidity and is generally in accordance with relative humidity forecasts. The quality of TAMDAR wind speed measurements is difficult to determine, however discrepancies between wind speed measured by radiosonde and TAMDAR can usually be explained to some degree by forecast or observed spatial variability in wind. It is concluded that implementing TAMDAR data into the observations and forecasting system of the IMO would nicely supplement traditional atmospheric soundings to increase the coverage and frequency of atmospheric measurements in Icelandic airspace.

Útdráttur

Háloftamælingar með veðurkanna (e. radiosonde) voru bornar saman við háloftamælingar framkvæmdar af TAMDAR yfir Keflavíkurflugvelli. Tilgangur verkefnisins var að meta mögulegan ávinning þess að innleiða TAMDAR-gögn í athugunar- og spákerfi Veðurstofu Íslands. Þrátt fyrir fremur lítið gagnasafn og mikinn breytileika í rúmi var ályktað sem svo, að hitamælingar TAMDAR væru áreiðanlegar og í góðu samræmi við hitamælingar veðurkanna. Niðurstöður verkefnisins benda til þess að vindáttarmælingar TAMDAR séu almennt góðar. TAMDAR nemur breytingar í loftraka og eru loftrakamælingar í samræmi við spár að allnokkru leyti. Gæði vindhraðamælinga TAMDAR eru torræð, en yfirleitt má skýra ósamræmi milli vindhraðamælinga veðurkanna og TAMDAR með þeim breytileika sem fram kemur í spám eða athugunum. Innleiðing TAMDAR-gagna yrði líkast til ágætisviðbót við þau gögn sem löngum hafa legið til grundvallar háloftaathugunum á Íslandi; slík viðbót yki víðfeðmi og tíðni háloftamælinga yfir Íslandi.

Contents

List of Figures

List of Tables

List of Acronyms

AMDAR Aircraft Meteorological Data Relay

ft feet

GS ground speed

hPa hectopascal

IAS indicated airspeed

ICAO International Civil Aviation Organization

IMO Icelandic Meteorological Office

kts knots

LSS local speed of sound

METAR Aerodrome routine meteorological report

NAWDEX North Atlantic Waveguide and Downstream Experiment

nm nautical miles

NWP numerical weather prediction

TAMDAR Tropospheric Airborne Meteorological Data Reporting

TAS true airspeed

UTC Coordinated Universal Time

WMO World Meteorological Organization

1 Introduction

Atmospheric sounding is essential to the analysis of meteorological conditions in the troposphere and to the assessment of cloud height, icing and general aviation weather conditions. Such information is of great importance to airmen and the aviation industry as a whole.

Traditionally, atmospheric soundings in Iceland have been performed by releasing radiosondes attached to a balloon up into the air so that it may measure various atmospheric parameters. As the balloon ascends, it expands and finally ruptures and falls to the ground. Ideally, it will reach an altitude of 80 to 100 thousand feet before this happens. Such atmospheric sounding methods require constant renewal of equipment as the balloons and their loads are disposable. Furthermore, man power is needed for their release and supervision. In the past decades, radiosondes have been launched from Keflavík airport every day at noon and midnight. Their associated measurements form a part of a global network of radiosonde soundings.

In recent years, efforts have been made to implement the employment of commercial aircraft to carry atmospheric sensors. In this way, the frequency of atmospheric measurements and the abundance of the associated data may be increased. Furthermore, no additional man power is needed for releasing the sensors into the air that way, no balloons or parachutes are needed to drive them up or break their fall and the coverage of data corresponds to the tracks flown by aircraft. Today, *Panasonic Weather Solutions* runs an extensive network of such measurements in collaboration with a number of airlines, one of which is *Icelandair*. The project is named Tropospheric Airborne Meteorological Data Reporting (TAMDAR) and has been in constant use and development since 2005, when the first TAMDAR sensors were fitted on aircraft owned and operated by Mesaba Airlines in the Great Lakes region in the USA (Mulally and Anderson, 2011).

This work was originally written as a B.Sc. thesis and published as such by the University of Iceland (Jóhannsson, 2016). Its aim is to assess the quality of data collected by TAMDAR in the vicinity of Keflavík International Airport and to compare them to data from traditional atmospheric soundings which have been practised by the Icelandic Meteorological Office (IMO) since 1952 and are described in more detail in Section 5.1. The radiosonde data were gathered by radiosondes from the IMO and North Atlantic Waveguide and Downstream Experiment (NAWDEX) in September and October 2016. The TAMDAR data were collected by Icelandair's Boeing 757 aircraft arriving at or departing Keflavík. Presently, the IMO does not use TAMDAR soundings routinely to assess conditions in the troposphere relevant to air traffic. This study seeks to evaluate to what extent TAMDAR data should supplement and/or replace data gathered with traditional radiosonde sounding methods in the assessment of aviation weather in Icelandic airspace.

2 The structure of the atmosphere

The atmosphere comprises the outermost part of the Earth system and consists of a mixture of gases, the greatest part of which is made up of nitrogen (78%), oxygen (21%), and water vapour in varying amounts (HMSO, 1994, p. 3 - 6). It extends from the surface of the solid Earth up to the exosphere, which ends at the vague boundary between Earth and space. The atmosphere, like any other part of the Earth system, is subject to Earth's gravitational attraction. Newton's universal law of gravitation, which is given by (1) below, states that the gravitational attractive force between two masses is inversely proportional to the square of the distance between them:

$$F = G \frac{m_1 \cdot m_2}{r^2},$$
(1)

where F is the attractive force between the two masses, G is the universal gravitational constant, m_1 and m_2 are the two masses and r is the distance between the masses (Newton, 1687). Thus, the atmosphere's average density and pressure are highest at Earth's surface and decrease almost exponentially with increasing height. Since pressure depends on both density and temperature, knowing the pressure on the ground is not enough to derive the exact air pressure at a given altitude. Instead, the temperature gradient (often referred to as lapse rate) of the atmosphere must be known as well. Equation (2) gives a good approximation of the pressure at altitude as a function of the pressure at a given reference altitude:

$$p(z) \approx p_0 e^{-\frac{z}{H}},$$
(2)

where $p(z)$ is the pressure at altitude z above the reference level, p_0 is the pressure at said reference level and H is a parameter, commonly named the *scale height*, which depends on temperature (Wallace and Hobbs, 2006, p. 9 and 69). To simplify the discussion of pressure variations with altitude, the International Standard Atmosphere was defined by the International Civil Aviation Organization (ICAO) in 1964 (HMSO, 1994, p. 6). It assumes an atmosphere with fixed pressure, temperature and density values at sea level and a fixed vertical pressure gradient and lapse rate. For any given pressure value, the height of the corresponding pressure level in the ISA is referred to as *pressure altitude*. Table 1 shows the approximate pressure altitude of various pressure levels.

The atmosphere is divided into a number of layers, based on variations in its temperature gradient as shown in Figure 1. These layers are referred to as *spheres* and their boundaries as *pauses*. In this context, the temperature gradient refers to the *average* change in temperature with increasing altitude.

The lowest layer of the atmosphere, and the most relevant one in the context of this work, is the *troposphere*. It is defined by a negative lapse rate and while its upper boundary, the *tropopause*, varies in altitude both seasonally and geographically, it generally lies between 8 and 18 km above sea level (HMSO, 1994, p. 4). The troposphere is both relatively dense and moist and as

Table 1: Height of pressure levels in ISA (HMSO, 1994, p. 7).

Height in ft	Pressure in hPa
55000	92
40000	188
35000	239
30000	302
25000	377
20000	466
15000	572
10000	697
5000	843
0	1013.25

a result, it is the regime of weather as we know it: clouds, icing, precipitation and wind. The troposphere is also the part of the atmosphere that accommodates the majority of commercial air traffic (National Research Council, 2001, p. 27). All the meteorological data considered in this work were gathered in the troposphere.

The *stratosphere* lies above the troposphere and starts where the temperature ceases to decrease with height. At the tropopause, the temperature reaches a local minimum of about -50 to $-60\,°C$. In the lowest layers of the stratosphere, it varies little but then starts to increase steadily with height up to the *stratopause* which is the upper boundary of the stratosphere. The stratopause lies about 50 km above sea level with a local maximum temperature of about $0\,°C$. These relatively high temperatures result from the presence of ozone, which absorbs much of the ultraviolet radiation reaching Earth from space (HMSO, 1994, p. 4 - 5).

Above the stratopause lies the *mesosphere*. In the mesosphere, temperature decreases again with height up to its upper boundary, the *mesopause*, where the atmosphere's temperature is at its lowest, at around -80 to $-100\,°C$. In the uppermost layer of the atmosphere, the *thermosphere*, the temperature increases with height. It is by far the most extensive one and does not have a well defined upper boundary. Its uppermost part is referred to as the exosphere and lies roughly 700 km above sea level (HMSO, 1994, p. 6).

As mentioned above, temperature gradients refer to the *average* change in temperature. Despite the troposphere being defined by a negative lapse rate, its temperature sometimes increases locally with altitude. This condition is referred to as a *temperature inversion*, or simply *inversion* (Wallace and Hobbs, 2006, p. 11).
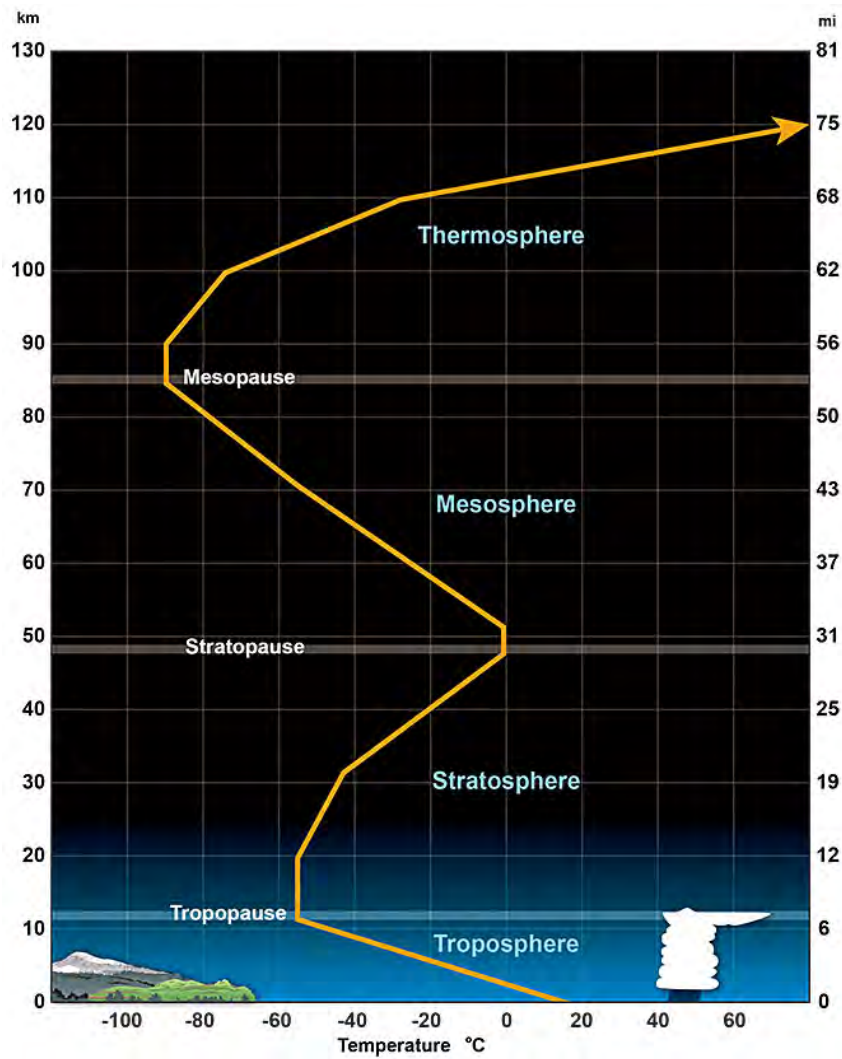
Figure 1: The different layers of the atmosphere defined by its temperature gradient (NOAA, 2016).

3 Atmospheric dynamics

3.1 Atmospheric forces and the movement of air

The atmosphere is a layer of gases resting on Earth's surface under its gravitational attraction. Because of Earth's motion in the solar system, its rotation about its own axis and the influence of the Moon and other planetary bodies on its gravitational field, everything belonging to the Earth system, including the atmosphere, is subject to a multitude of forces. Atmospheric dynamics seek to explain and understand, among other things, the weather phenomena observed on Earth in terms of these forces and the resulting motion of the atmosphere relative to Earth's surface.

Local pressure variations in the atmosphere are among the driving forces of weather. A *high pressure system*, or *high*, refers to an atmospheric pressure anomaly that results in a local maximum of atmospheric pressure at the surface. Similarly, a *low pressure system*, or *low*, refers to an anomaly that results in a local pressure minimum on the ground. On a hypothetically stationary Earth, air would flow directly from areas of high pressure towards areas of low pressure until the pressure variations were eliminated. In this scenario, the only force acting on the air would be the *pressure gradient force*. However, because of Earth's rotation, another force acts on air moving across its surface. In a reference system fixed to Earth's surface, this force seeks to deflect the trajectory of any mass travelling across it to the right in the northern hemisphere, but to the left in the southern hemisphere. It is called the *Coriolis force* after the french mathematician G.G. Coriolis, and is given by the equation:

$$F_C = -2\Omega V sin(\phi), \tag{3}$$

where Ω is the angular velocity of Earth, V is the velocity of the mass relative to its surface and ϕ is the geographic latitude (Barry and Chorley, 2010, p. 146). From (3), it can be seen that the Coriolis force is strongest at Earth's geographic poles but decreases towards the equator, where it is non-existent. At the site of this study, on a latitude of about 64°N, the contribution of the Coriolis force is significant.

From the discussion above, it is clear that in the northern hemisphere, air travelling away from a high is deflected to the right so that an anticlockwise flow pattern around its center is established when viewed from above. Such high pressure systems are commonly referred to as *anticyclones*. Air moving towards a low under the pressure gradient force is also deflected to the right on its way and thus tends to follow a clockwise circular path around the center of the low when viewed from above. Such low pressure systems are commonly referred to as *cyclones*. Figure 2 shows a schematic of air moving under the pressure gradient force and the Coriolis force in the northern hemisphere.
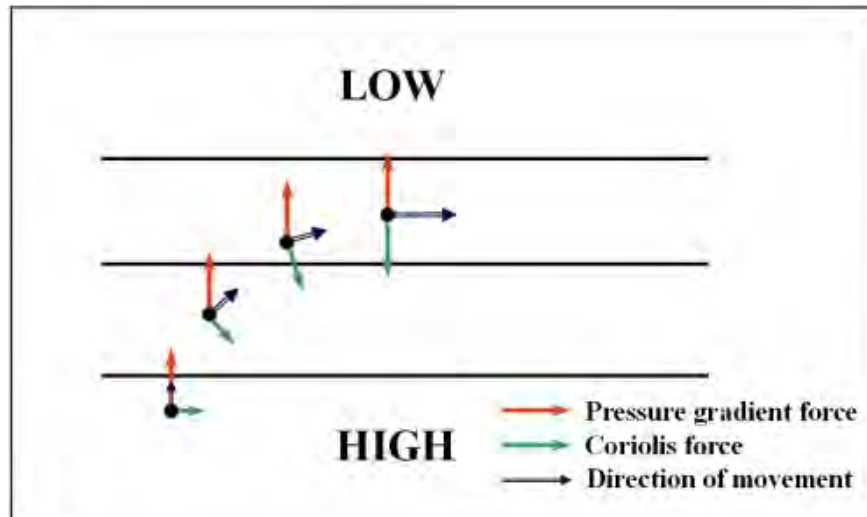
Figure 2: Schematic picture of air moving under a pressure gradient force and Coriolis force in the northern hemisphere (Leung, 2016).

More forces than the pressure gradient force and the Coriolis force act on air travelling across Earth's surface. Frictional forces play an important role in the movement of air. Since the atmosphere is in contact with the surface, it experiences friction at the boundary. Frictional forces reduce the velocity of the air. As the Coriolis force is proportional to velocity, friction reduces the deflection of the air due to the Coriolis force whereas the pressure gradient force remains unaffected. Therefore, the overall effect of friction on air moving under influence of the Coriolis force in the northern hemisphere will be to deflect it to the left, towards the center of the low. Air at low altitudes, closer to the surface, experiences more friction than air at higher altitudes. Thus, with increased altitude, wind tends to strengthen and to flow increasingly parallel to isobars. In the northern hemisphere, this means a clockwise veering (as viewed from above) of the wind with altitude. Air travelling over a smooth surface, such as the sea, experiences less friction than air travelling over mountainous terrain, densely populated areas or areas of dense vegetation. Wind speed and wind direction vary depending on the surface over which the wind is blowing (Barry and Chorley, 2010, p. 145 - 150).

3.2   Mid-latitude weather fronts and the Norwegian Cyclone Model

An air mass is defined as an expanse of air that has characteristic properties resulting from its present or prior residence over some geographic region (Wallace and Hobbs, 2006, p. 375). An important characteristic of air masses, which governs many of their other properties, is their temperature. As an example, consider air which has rested over the North Pole for some period of time. As a result of its underlying ice sheet, this air will become relatively cold. When it moves southwards, say, towards the Atlantic, its temperature will remain relatively low for some period of time, thus making it distinguishable from warmer air which has been resident over the Atlantic Ocean. Weather fronts are defined as the boundary between two air masses. When the temperature gradient across a front is high, the front is said to be strong. Similarly, if there is relatively little temperature variation across the front, it is said to be weak. On surface weather

charts, fronts are drawn according to their position on the ground. They do not extend vertically upwards from the ground, rather follow a slope which varies depending on conditions, and this should be taken into account when using weather charts for analysis.

Between approximately 40° and 70° N, a complex pattern of moving high and low pressure systems prevails. In this band, which is often referred to as the westerly belt because of a predominantly westerly airflow aloft, cold air from polar regions meets warmer air from more temperate regions. The boundary between the cold and the warm air is called the *polar front* and along this front, formation of dynamic weather systems is a regular occurrence. The dominant westerly circulation associated with the polar front can reach speeds of up to 270 kts in the winter. The narrow ribbon where it reaches its highest speeds is referred to as the *jet stream*. It is commonly discontinuous or split and varies in location, like the polar front itself (Barry and Chorley, 2010, p. 5 and p. 171 - 172).

A well-studied and common phenomenon in the westerly belt is the *mid-latitude depression* which is commonly associated with the convergence of air masses. The formation and development of this weather system is described by the *Norwegian cyclone model*. According to this model, the boundary of the two air masses assumes the shape of a wave, which then propagates eastwards. It encloses a sector of relatively warm air between two colder air masses and a cyclonic low pressure system forms. The atmospheric wave is made up of two fronts: a warm front which precedes it and a cold front which succeeds it. At the cold front, a cold air mass moving eastwards forces a warmer air mass ahead of itself. Since the cold air is denser than the warm air, it tends to flow underneath the warmer air, thus lifting it. This causes large scale convection and unstable atmospheric conditions which frequently result in shower formation and associated precipitation. At the warm front, the warm air mass pushes a colder air mass ahead of itself, resulting in stable atmospheric conditions. As the warm sector cools at its boundary to the colder air mass, it contracts and its moisture capacity lessens. Layered clouds and continuous precipitation are often associated with warm fronts. Once the atmospheric wave has developed into a cyclone, the cold front catches up with the warm front and the resulting front is said to be occluded. The formation and progression of a mid-latitude cyclone is shown in Figure 3a (Barry and Chorley, 2010, p. 226 - 244).

As the cold front catches up with the warm front, the two colder air masses, which enclose the warm sector, force the warm air between them upwards. The forced rising of the warm air encompasses convective activity which is characterized by vertical cloud formation, windy and gusty weather and precipitation. A schematic drawing of the cross section of an occlusion is depicted in Figure 3b. Note that the progression and symptoms of the cyclone described here are not universal. They depend on the strength of the fronts as well as the presence of other weather systems influencing the state of the atmosphere. However, this model is useful for understanding the general formation and development of mid-latitude cyclones, which are a relatively common occurrence in Iceland (Barry and Chorley, 2010, p. 226 - 244).

[From *Extratropical Cylones: The Erik Palmen Memorial Volume*, Amer. Meteorol. Soc. (1990) p. 188.]
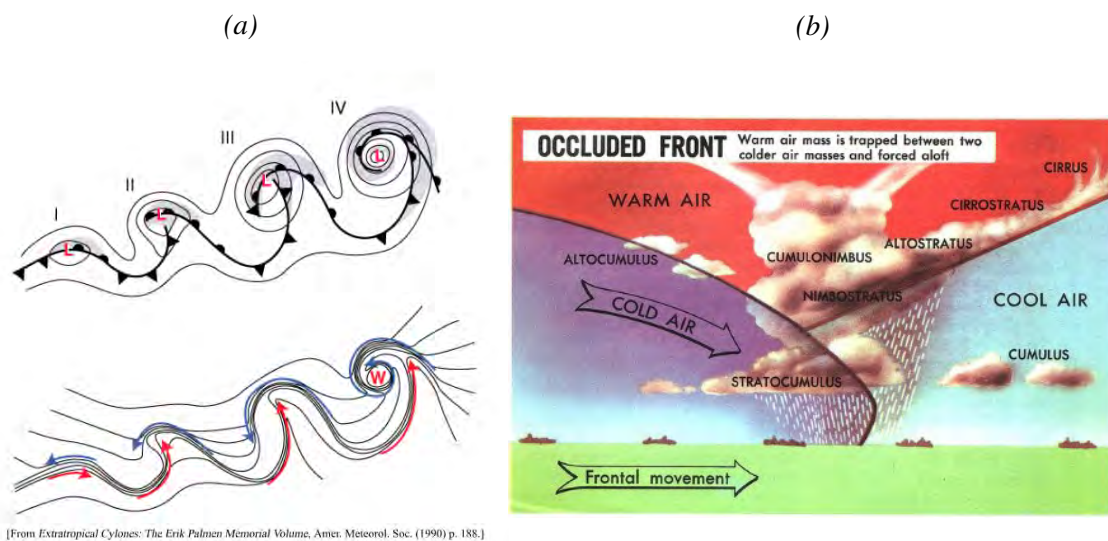
Figure 3: (a) The formation and progression of a mid-latitude cyclone according to the Norwegian cyclone model (Wallace and Hobbs, 2016, p. 336) and (b) a schematic drawing of the cross section of an occluded front and the associated weather conditions (EUME-TRAIN, 2016).

4   Aviation meteorology

Aviation meteorology is a branch of meteorology relating to atmospheric conditions relevant to air traffic. It addresses weather conditions in the whole troposphere and phenomena which affect aircraft passing through it. Some of the weather present at altitude does not directly affect conditions at ground level and may even go undetected by people on the ground. However, such high altitude phenomena can be of great relevance to airmen and the aviation industry. Examples include the formation of icing on airframes, turbulence, high clouds and winds aloft, both lateral and vertical, including mountain waves and jet streams.

Due to the somewhat different emphasis of aviation meteorology to surface based meteorology, and due also to the difference in the target groups of information relating to those two fields, weather forecasts and observations in aviation meteorology are supplied and set forth in a different way to what a layman may be used to. These information are closely tailored to the needs of aviators, and put forward on a format that seeks to optimize their value for airmen while minimizing their size, since they need to be transferred quickly and efficiently between their issuers and their end users. Pilots are trained in assessing weather conditions aloft and in reading and using information published in this way.

One format which is commonly used for reporting weather observations at a specific aerodrome is the so called *Aerodrome routine meteorological report (METAR)* (ICAO, 1998). Figure 4 shows an example of a METAR report from Reykjavík airport. Despite its short length and modest presentation, this weather report contains information about the time and place of observation, the mean and gusting wind speeds, the wind direction, visibility, weather, height and coverage of cloud layers above the airfield as well as the local temperature, dew point and air pressure. A commonly used code word in METAR is *CAVOK*, written in capital letters. It means that "cloud **C**eiling **A**nd **V**isibility are **OK**" and implies a visibility of 10 km or more, an absence of clouds below 5000 ft and an absence of weather significant to air traffic at the airfield. For further information on METARs and other aviation weather reporting formats, refer to Part A of the World Meteorological Organization (WMO) *Manual on codes* (WMO, 2014).

BIRK	2016-11-08 13.00	METAR BIRK 081300Z 21018G28KT 9999 VCSH FEW017 BKN031 BKN060 04/M01 Q0984

Figure 4: METAR report for Reykjavík airport issued on 8 November 2016.

The history of powered flight began in North Carolina in 1903 with the Wright brothers (Batchelor and Lowe, 2006, p. 34 - 35). Modern aviation is still marked by its geographical and historical origin in that the use of SI (Système International) measuring units is not widespread in aviation, despite an effort to implement their use (ICAO, 2010). Most of the aviation industry still refers to altitude in terms of feet (ft), speed in terms of knots (kts) and distance in terms of nautical miles (nm). The units used in this work, as in aviation meteorology and the aviation industry in general, will often be in accordance with these customs. Air pressure will be stated in hectopascal (hPa), which is equivalent to the historically more commonly used millibar. Time will be given in Coordinated Universal Time (UTC), which is also the zonal time in Iceland all year round.

5   Atmospheric profiling

Atmospheric profiling is an important field of meteorology which addresses the measuring of various parameters of the atmosphere to construct a clear picture of how its temperature, pressure, humidity, density and other characteristics vary spatially and temporally. Many methods need be employed to construct this picture, and Figure 5 shows an artist's impression of a few of those methods. Some of them, such as on-shore and off-shore synoptic weather stations, are suitable to survey the atmosphere at ground level, while others, such as some satellites which employ remote sensing techniques, may be suitable for the highest layers of the atmosphere, depending on conditions. Radiosondes and TAMDAR are used for surveying of the troposphere.
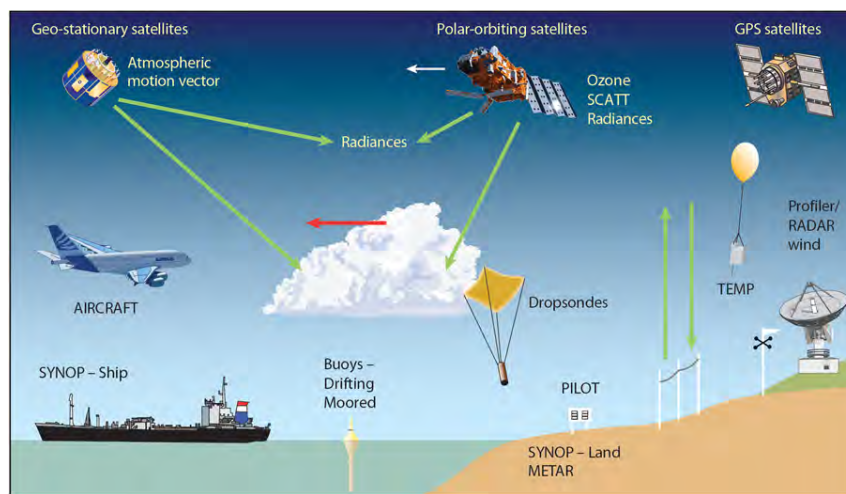

Figure 5: Artist's impression of the various methods used to measure atmospheric conditions (ECMWF, 2016).

Of all the methods that are used for measurements in the atmosphere, each one has its advantages and disadvantages. While some devices, such as certain types of satellites, are able to capture a relatively large portion of Earth's surface in a relatively low resolution, others, such as traditional weather stations, can only sample atmospheric parameters at a single location and thus cannot account for spatial variability in the atmosphere. However, weather stations on the ground can produce long time series and give an excellent picture of temporal variability of the parameters that they measure. Radiosondes are rather confined in their lateral movement but have a good vertical reach. TAMDAR is usually more constricted in the vertical while sampling a relatively vast lateral portion of the atmosphere, as the commercial aircraft that carry it travel relatively long distances but normally spend most of the flight at a constant cruising altitude. The fact of the matter is that the spatial and temporal resolution of different methods and devices vary greatly and thus a combination of many methods is necessary to establish as accurate a picture of the state and variability of the atmosphere as possible.

Aircraft have been surveying the atmosphere since before the beginning of commercial aviation. Most aircraft are equipped with some instrumentation and nowadays, all commercial aircraft are subject to a rigid body or rules and regulations prescribing the proper installation and use of a wide variety of advanced instrumentation. Commercially operated aircraft are legally required to carry sensitive pressure altimeters, thermometers indicating outside air temperature and pre-

cise navigation instrumentation (ICAO, 1998). These regulations are the product of an almost world wide common effort to increase air safety by making information on the meteorological conditions in the immediate vicinity of an aircraft readily available to the pilots operating it. Other aircraft based observing systems that utilize aircraft on board sensors include the Aircraft Meteorological Data Relay (AMDAR) observing system which was implemented by the WMO in 1998 (WMO, 2016).

Surveying the atmosphere with commercial jet powered aircraft does pose some challenges connected to their operational environment. At Icelandair, the Boeing 757 typically cruises between 30 and 42 thousand feet at 76 to 83 percent the speed of sound (Hallgrímur Jónsson, personal communications, 7 December 2016). Measuring airspeed, pressure and temperature at such velocities is all but straight-forward. As the aircraft penetrates the air in its immediate vicinity, it causes pressure disturbances in it and produces both turbulent and laminar flow on and around its airframe. The internal movement of the air particles caused by the airframe-induced disturbances, as well as the direct contact of air with the airframe itself causes frictional heating of both the air and the airframe. The compression of air in the aircraft's path also becomes a significant factor at cruising speeds of jet powered aircraft. Compression waves are generated around the aircraft and at speeds close to the speed of sound, these compression waves cause considerable heating. Accurately measuring the atmosphere's actual temperature and pressure so close to these heat-generating pressure waves requires smart design and exact calibration (Oxford Aviation Academy, 2011, p. 407 - 422 and p. 442).

As simple as the concept of speed may seem, measuring it can pose some challenges in the environment where aircraft operate. To discuss speed, a reference has to be defined. The aircraft's speed relative to the air that it moves in is referred to as indicated airspeed (IAS) in aviation. It is the speed at which air passes over the aircraft's control surfaces and determines its performance and controllability and is thus of utmost importance for pilots and aircraft manufacturers. To assess the time it takes to fly a certain distance, including climbs and descents, the indicated airspeed is not suitable at all. For straight and level flight, the speed at which the aircraft passes over the surface, commonly referred to as ground speed (GS), should give a better estimate. However, the indicated airspeed can be corrected to give an accurate true airspeed (TAS) of the aircraft. Theoretically, this is the actual speed of the aircraft through space; it is the speed on which distance and time calculations are based in the aircraft. Finally, the *Mach number* denotes the ratio of the TAS to the local speed of sound (LSS) and is commonly used to measure airspeed at speeds that are close to the LSS. The speed at which sound waves move through a gas is proportional to the square root of the specific heat ratio of the gas and its absolute temperature as stated by (4) below.

$$M = \frac{TAS}{LSS} = \frac{TAS}{\sqrt{\gamma RT}},$$
(4)

where $\gamma = \frac{C_p}{C_v}$ is the specific heat ratio (about 1.4 for air) and R is a constant specific to the gas in question (about $287 \frac{J}{kgK}$ for dry air) (Crocker, 1998, p. 62).

5.1 Radiosondes

Figure 6: Sigurjón Gestsson, duty officer at the IMO, releases a weather balloon in Keflavík in 1974. Photo credit: Guðmundur Ingólfsson.

The term *radiosonde* refers to a balloon-borne instrument that transmits atmospheric data to a receiver on the ground (DuBois et al., 2002, p. iv). The origin of the radiosonde dates back about one hundred years. During World War I, it became clear that information about winds aloft would be of great value for operators of military aircraft, facilitating both navigation, precise artillery fire and chemical warfare. Ascending balloons could be tracked using theodolites during hours of daylight and good visibility but at night or when low visibility prevailed, such methods would be of little use. Towards the end of the war, experimentation with wireless transmission of radio signals from airborne spark transmitters had begun in Germany. Since the first successful tracking of airborne radio transmitters, conducted by Colonel William Blair in Ohio in the early 1920s, radiosondes have revolutionized the survey of the atmosphere and have made an immensely important contribution to atmospheric science and meteorology (DuBois et al., 2002, p. 26 - 29). The IMO has practised regular atmospheric soundings since 1952 (Garðarson, 1999, p. 139 - 142). Figure 6 shows a traditional radiosonde launch.

Modern radiosondes combine highly advanced instrumentation with precise positioning technology and measure various parameters. The models used in this study are the two latest radiosonde productions from Vaisala. The Vaisala RS92 was used by the IMO whereas a more recent model, the Vaisala RS41, was used by NAWDEX. Both of these devices transmit their data digitally in one second intervals. They use the same measurement principles: a platinum resistance sensor to measure temperature and a twin film capacitor to measure relative humidity. They employ GPS to determine height and position as well as to calculate wind and pressure values. The variables measured by the radiosonde are shown in Table 2. Note that winds can be logged either in kts or m/s depending on user preference (Vaisala, 2010 and 2016).

Table 2: Variables logged by the radiosonde.

Variable	Unit
GPS altitude	ft or m
Air pressure	hPa
Temperature	$°C$
Wind speed	kts
Wind direction	$°$
Lateral wind component	kts or m/s
Vertical wind component rate	kts or m/s
Relative humidity	%
Rate of ascent	m/s

The radiosonde is driven upward by a helium or hydrogen filled balloon which it is attached to via a 30 m long suspension string. An unwinder is fitted to unwind the string gently when the sonde is launched. The device is powered by batteries and its measurements can be monitored in real time during its ascent with a designated software. Optimally, the device will transmit measurements for two hours or more before the battery runs out or the balloon ruptures and the device falls to the ground. Some radiosondes are fitted with parachutes to break their fall. Some employ a radar reflector to facilitate the detection of the radiosonde on primary radar (Vaisala, 2010 and 2016). Figure 7 shows different configurations of the Vaisala radiosonde.
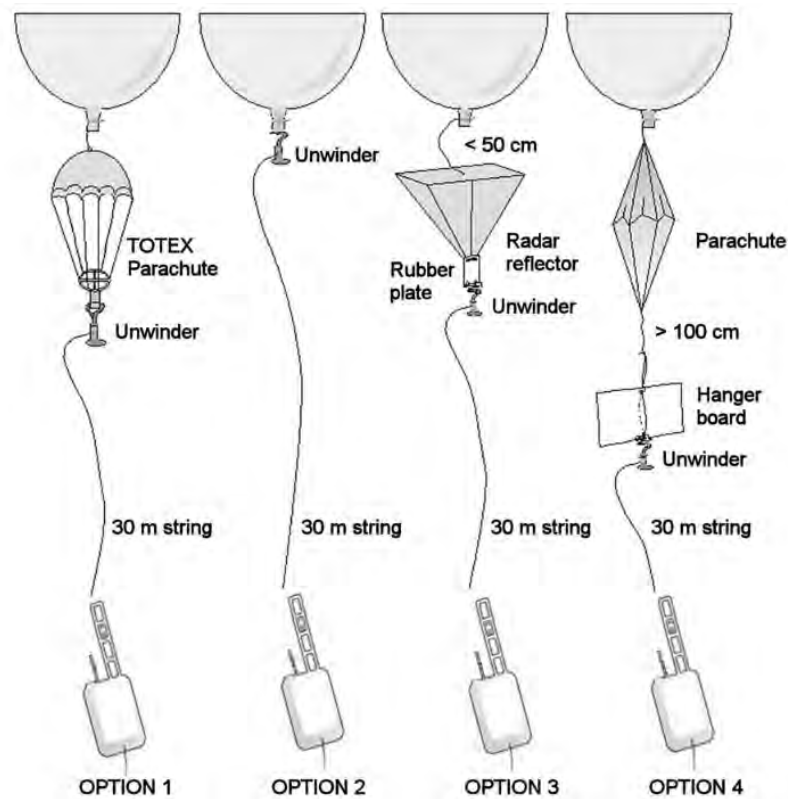

Figure 7: Four different radiosonde assemblies (Vaisala, 2010).

5.2 TAMDAR

The TAMDAR probe is wing shaped and designed to be aerodynamically efficient. The probe is attached to a box which includes the data acquisition and signal processing hardware and software. This combination is called the TAMDAR sensor. Like the radiosonde, it measures different variables and transmits its measurements digitally in real time (Daniel Mulally, personal communication, 2 December 2016). The parameters measured by the TAMDAR sensor that are relevant in this study are displayed in Table 3. A schematic drawing of the probe's interior is shown in Figure 8. Temperature measurements are made with a resistive temperature device. Total ram pressure is measured by the pitot pressure port on the probe's leading edge and static pressure at its trailing edge (Daniels, 2002). Theoretically, the difference in total ram and static pressure amounts to total dynamic pressure, from which, after application of various corrections and taking into account the local air temperature, the TAS can be derived. As explained in this Chapter, the Mach number can then be derived from TAS and the temperature by (4).

Table 3: Variables logged by TAMDAR relevant to this study.

Variable	Unit
Pressure altitude	ft
GPS altitude	ft
True Airspeed (TAS)	kts
Temperature	°C
Wind speed	kts
Wind direction	°
Icing	ice/dry
Relative humidity	%

The wind is calculated using input from the pressure sensors of the TAMDAR and from its built-in GPS. By measuring the GS of the aircraft and its TAS, as well as comparing the ground track with the actual heading of the aircraft (commonly referred to as air track), both wind speed and wind direction can be calculated. The following vector equation describes this relationship in a simple way:

$$\vec{W} = \vec{G} - \vec{A}, \tag{5}$$

where $\vec{W}$ refers to the wind itself, $\vec{G}$ to the ground track and $\vec{A}$ to the air track (Mulally and Anderson, 2011).

Relative humidity is measured directly using two capacitive sensing devices. This has proven to yield good accuracy with great operational simplicity and limited need for maintenance (Mulally and Braid, 2009). The humidity sensors, along with the RTD temperature sensor, are located within the so-called sensing cavity into which outside air is fed through the flow tube. The flow
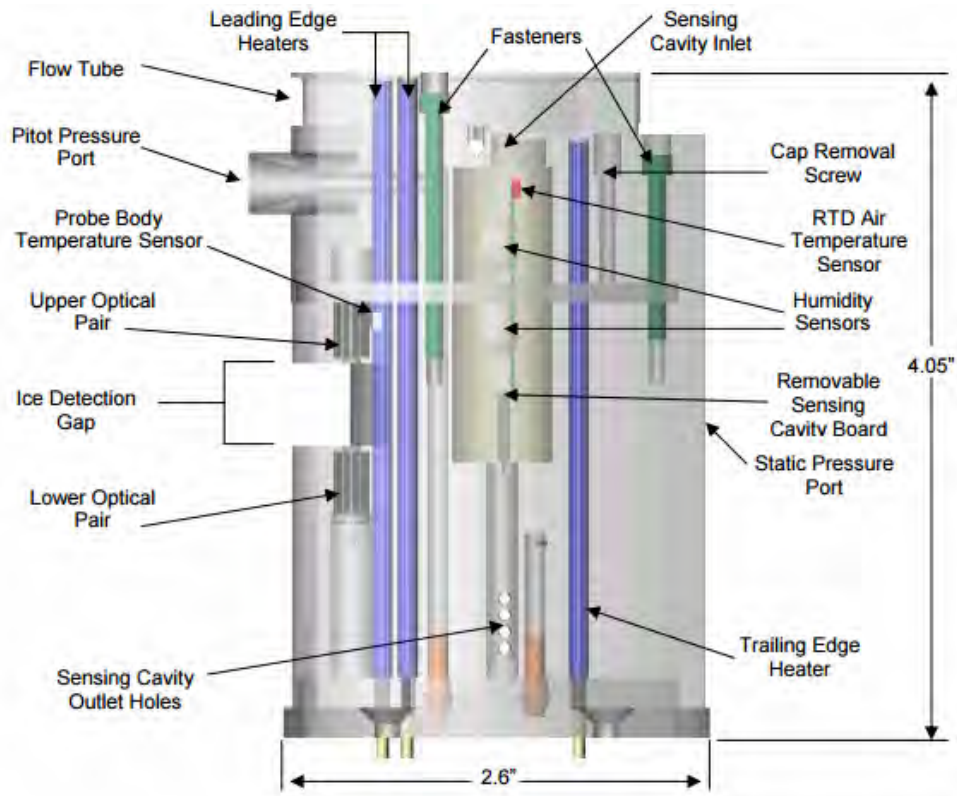
Figure 8: A schematic overview of the interior of the TAMDAR probe (Daniels, 2002).

tube opening is located at the outer leading edge of the device, where the distance to the airframe is greatest so as to minimize airframe induced disturbance of the air. The air then flows out of the sensing cavity through the outlet holes, where the pressure is at its lowest (Daniel Mulally, personal communication, 2 December 2016).

Detection of ice is carried out by optical sensors on each side of the ice detection gap, which is located about midway across the leading edge of the probe. When icing is detected, the probe's own internal heating system is activated to melt the ice. This renders most measurements unreliable and under such circumstances, the sensor does not generally log its measurements. Of the measurements analyzed in this study which reported icing within the area of interest, only about 1% reported values for both wind, temperature and relative humidity. The TAMDAR data analyzed here do not include any icing scenarios - all of the data considered here have been collected under ice-free conditions. Figure 9 shows a TAMDAR probe in its operational environment, mounted on an aircraft.

Figure 9: A TAMDAR sensor installed on the airframe of a jet aircraft (Panasonic, 2016).

6 Data

The TAMDAR data used in this study were collected by Icelandair's Boeing 757 aircraft. Icelandair operate out of Keflavík airport, which is the largest international airport in Iceland. The airport is located close to the western tip of the Reykjanes peninsula. The peninsula is mostly made up of bare lava fields. It is mountainous and hardly vegetated.

Of the TAMDAR data used in this work, all of which were registered within the area in Figure 10, about one third proved complete; two thirds of the data did not contain measurements for all the parameters that were to be analyzed. A part of the incomplete cases result from icing conditions, in which measurements are often rendered unreliable and not registered, as explained in Chapter 5.2, but the reason for measurement failure outside of such condition was not researched particularly and is thus unknown.

Generally, the tracks of the radiosondes and the TAMDAR equipped aircraft do not coincide spatially. The balloons ascend at around 15 ft/s and are carried with the wind. Their trajectory gives a good indication of how wind direction and wind speed changes with altitude. Aircraft generally land and take off into the surface wind at the airfield, as far as runway availability permits, and fly approach and departure tracks according to instructions from air traffic control. In this work, only TAMDAR data registered in the area shown in Figure 10 is considered. It is assumed that if these data were logged within an hour before the release of the radiosonde and an hour after cessation of a radiosonde's measurements, the two datasets (TAMDAR and radiosonde) are eligible for comparison. Weather forecasts and observations from the time periods of the data in question will be used to analyze the state of the atmosphere during collection of the data.

It should be noted, that in the period that the data were gathered, runways 01 and 19 (lying in a north-southerly direction) at Keflavík airport were closed for maintenance and thus, all aircraft arriving at and departing the airport were bound to use the perpendicular runways 11 and 29. It should also be noted, that whereas radiosondes are usually released twice per day as mentioned in Chapter 1, more sondes were released from Keflavík during the period 27 September to 14 October 2016 due to a field campaign of a multinational tropospheric research project called NAWDEX (North Atlantic Waveguide and Downsteam Impact Experiment) in Iceland. Both NAWDEX and the IMO released additional sondes during this period and the NAWDEX group graciously offered all of their data to the IMO for analysis and comparison with TAMDAR data.

Five different days were selected for comparison analysis. The selection of those days was based mainly on the availability of TAMDAR data that had been collected within the time periods assigned to the radiosonde launches, as described in this chapter. Various images were prepared to facilitate a visual comparison between TAMDAR and radiosonde data. To allow single TAMDAR-missions to be distinguished, each aircraft was assigned one colour that represents the trajectory of the corresponding TAMDAR flight in the figures in Chapter 7. The aircraft registration numbers and their corresponding colours are displayed in Figure 10.
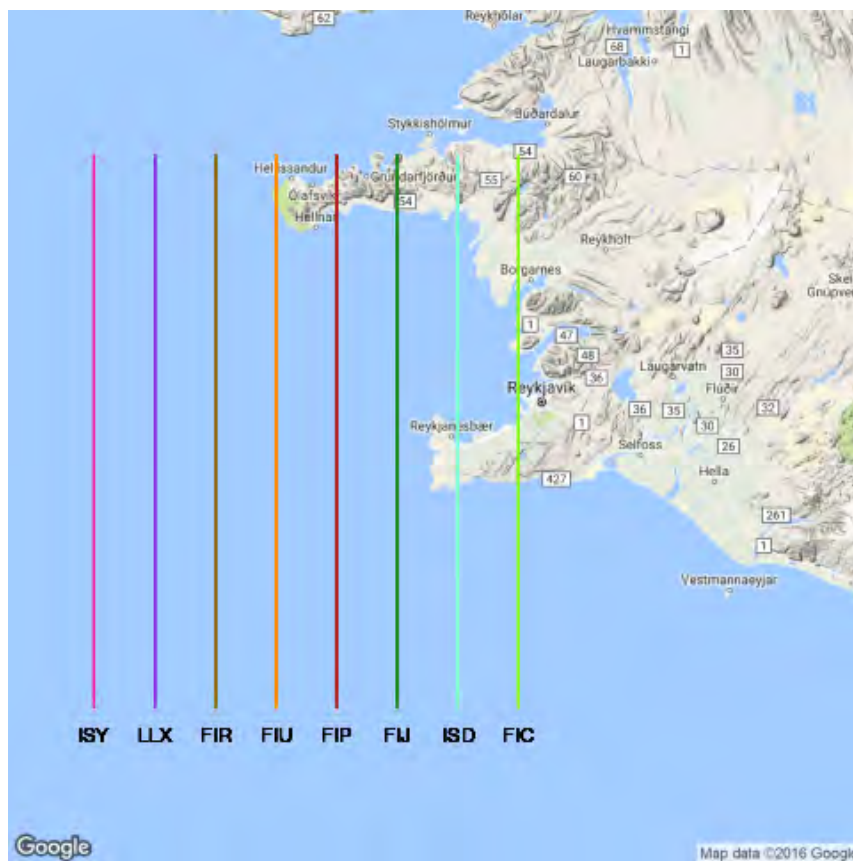
Figure 10: The airspace of interest and the colour representation of different TAMDAR carrying aircraft. The three letter identification corresponds to the last three letters in the aircraft's registration number.

7 Results and discussion

Data analysis and production of plots were carried out with the statistical computing and graphics tool **R**. Statistical calculations were done with the stats package (R core team, 2016). The analysis is based upon a comparison of the vertical profiles of TAMDAR and radiosonde for temperature, wind speed, wind direction and relative humidity. The time and distance between the compared measuring points varies and is significant. In this chapter, five different cases are discussed, see Table 4. A variety of weather charts are used to review the weather conditions in each case and to assess how the spatial and temporal variability of the parameters of interest affect the results of the comparison analysis. The charts represent either synoptic weather observations or numerical weather prediction (NWP) model output. All weather charts are produced by the IMO except otherwise stated. At the end of this chapter, the effect of the distance and time between the measuring points on the analysis will be discussed.

Table 4: An overview of cases analyzed (September - October 2016).

Case	Day	Time span (UTC)	No. of aircraft	No. of logs
1	27 September	15:54 to 17:44	7	80
2	29 September	16:57 to 17:53	4	32
3	1 October	16:23 to 17:59	5	36
4	2 October	13:25 to 15:55	5	36
5	27 October	23:15 to 23:48	2	37

7.1 Case 1 - 27 September 2016
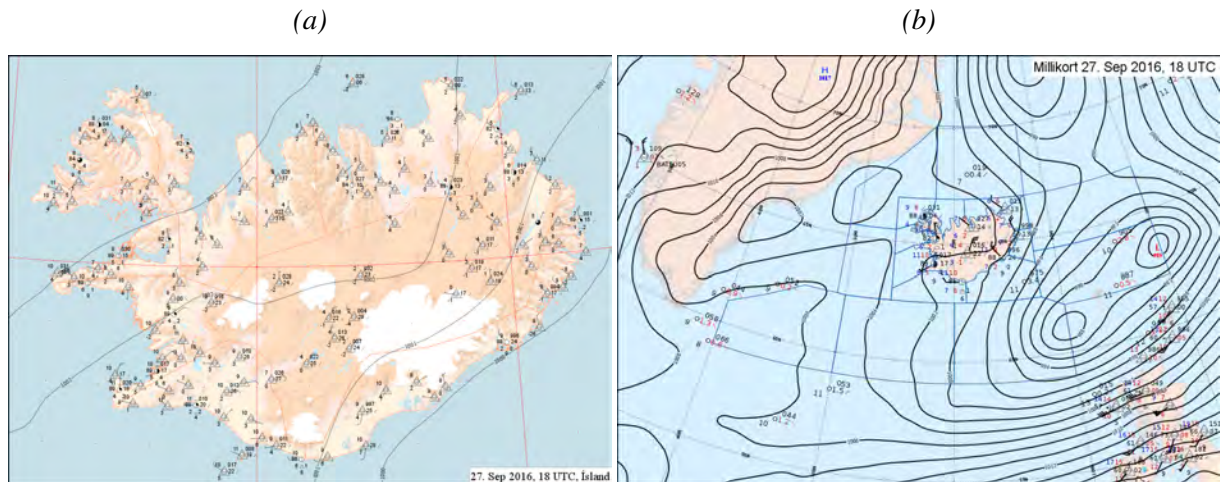
The weather situation

Figure 11: Synoptic weather charts for (a) Iceland and (b) the northern North Atlantic valid at 18 UTC on 27 September 2016.

On 27 September 2016, a high pressure ridge built up over the Irminger Sea, between Greenland and Iceland, and calm weather conditions set in over Iceland. Between 17 and 22 UTC, Keflavík METARs reported northerly winds at 6 to 8 kts, CAVOK, and a gradual rise in air pressure. According to synoptic weather charts, the center of the weak high pressure system reached Iceland in the evening and remained over Iceland until the early morning hours the next day. This type of weather system is called a *temporary cold anticyclone*. It is a region of relatively dry and cold air between two eastbound low-pressure systems. Since Iceland is located close to the Polar front in the path of many eastbound low pressure systems travelling across the North Atlantic, this weather phenomenon is commonly observed there. It brings a short period (often about one day) of dry weather between the wetter, more dynamic weather conditions connected to the previous and the subsequent low (HMSO, 1994, p. 270). Anticyclonic conditions like those described above are characterized by relatively calm winds and a well layered atmosphere. Figure 11 shows synoptic charts for Iceland and the northern North Atlantic at 18 UTC.

The measurements

A NAWDEX radiosonde was released from Keflavík airport at 16:54 UTC and 80 measurements from seven different TAMDAR equipped aircraft were selected for comparison. Table 5 shows the number and time frame of the measurements broken down by airplane. The trajectories of the TAMDAR flights are shown in Figure 12. In this case, three of the aircraft followed almost identical tracks to the west of the airport. This is not uncommon, since aircraft arriving or departing controlled airports are often directed to fly predetermined approach or departure procedures.

Table 5: An overview of TAMDAR measurements within the airspace shown in Figure 10 associated with the radiosonde launched at 16:54 UTC on 27 September. Measurements are broken down by airplane with the times of the first and last measurement of each plane along with the number of measurements of each plane information on whether each plane was departing or arriving at the airport.

Aircraft	First log	Last log	No. of logs	DEP/ARR
ISD	15:54	16:08	8	ARR
FIC	15:55	16:08	8	ARR
ISY	16:36	16:51	14	DEP
FIP	17:02	17:14	14	DEP
FIU	17:05	17:17	14	DEP
LLX	17:18	17:33	17	DEP
FIJ	17:34	17:44	5	DEP

Figure 12: The tracks of TAMDAR flights (coloured) registered within the airspace shown and in the time frame of the radiosonde launched at 16:54 UTC on 27 September 2016, along with the trajectory of the radiosonde (black).

Figure 13 shows a comparison of temperature measurements. Despite the great spatial variability of the data, its correspondence is very good.
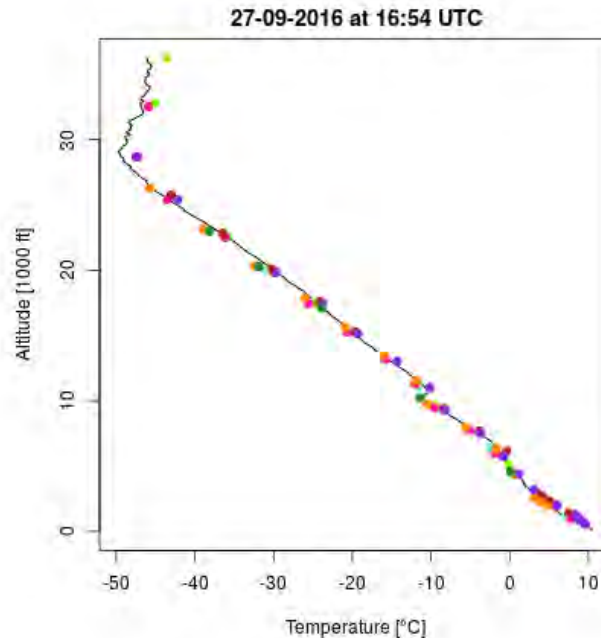

Figure 13: The temperature profiles of the radiosonde along with TAMDAR temperature logs from 27 September 2016. The colours of the TAMDAR points correspond to the aircraft as shown in Figure 10.

Measured wind speed is compared in Figure 14a. The wind measurements of the TAMDAR are reasonably consistent with those of the radiosonde, especially below 12 thousand feet. Above 20 thousand feet, the measurement values diverge. Above 28 thousand feet, the sonde reports a steep increase in wind speed and the TAMDAR captures this increase; in fact, four out of the five TAMDAR measurements above 28 thousand feet follow the profile of the radiosonde. Figure 14b compares the measured wind direction. Points of wind speeds less than 10 kts are not shown in the figure, as wind direction measurements at such low airspeeds are not reliable. Most TAMDAR wind direction measurements fall into a similar direction as the radiosonde logs. Since the last METAR before the release of the radiosonde reported winds veering through 80 degrees (this veering is not seen in the figure due to low associated wind speed), and because of the relatively great variability in wind direction throughout the afternoon, further analysis and discussion of wind direction measurements for this case will be refrained from.

(a)   *(b)*
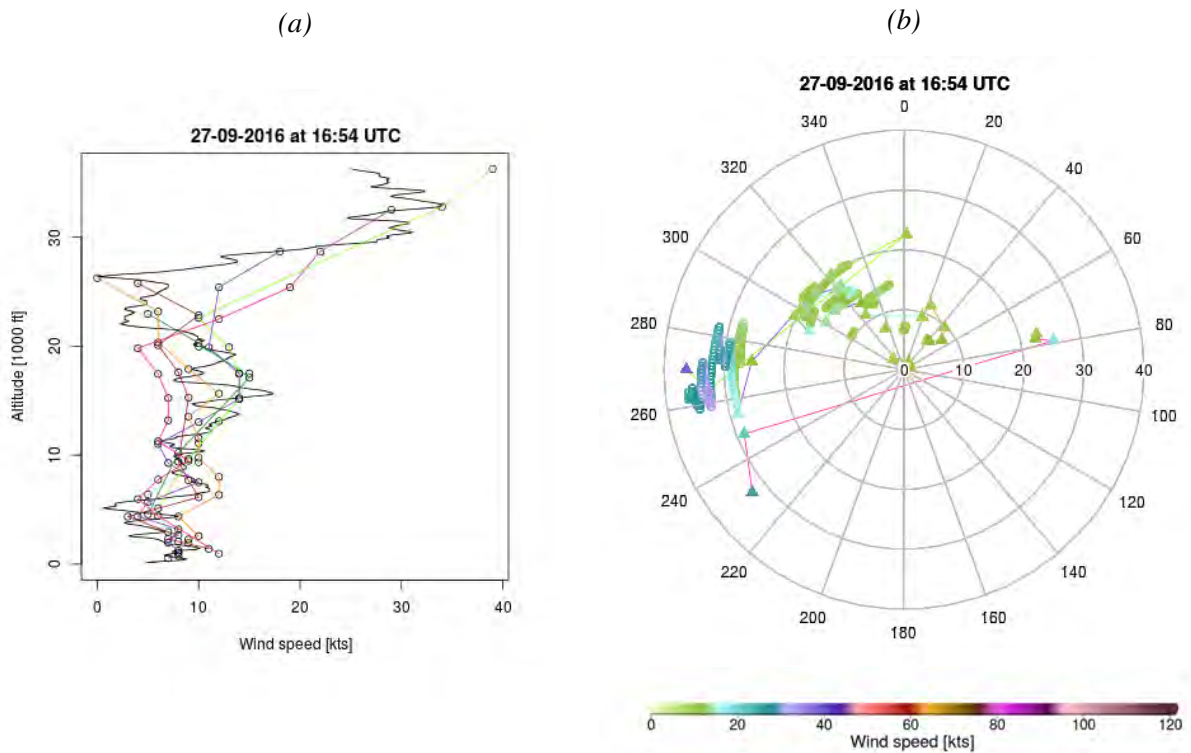
Figure 14: (a) Wind speed profile of radiosonde (black) and TAMDAR (coloured) and (b) wind direction profile of radiosonde (circles) and TAMDAR (triangles and lines) on 27 September 2016. In (b), the radial axis represents altitude in thousands of feet while the angular axis represents wind direction in degrees. The colour scale applies to the wind speed shown by the triangles and the circles. Wind measurements of less than 10 kts have been removed. In both (a) and (b), the colour of the lines connecting TAMDAR measurements are in accordance with Figure 10.

23

A comparison of relative humidity is shown in Figure 15. Below 10 thousand feet, the radiosonde and the TAMDAR are highly consistent. The general tendency of the TAMDAR seems to be to overestimate the relative humidity as measured by the sonde, and this tendency strengthens with increased altitude. The fact that the total distance between the sonde's and the TAMDAR's measuring points also increases with height, might (and should, at least to some degree) explain this trend. It should come as no surprise that the overall consistency of the TAMDAR data itself generally decrease with height, since the distance between aircraft flying different procedures increases with altitude. The consistency of the relative humidity measurements, when compared to, say, the temperature, is quite poor. In fact, the consistency of the temperature measurements is rather striking, considering the great spatial (and less significant temporal) variability of the measurements.
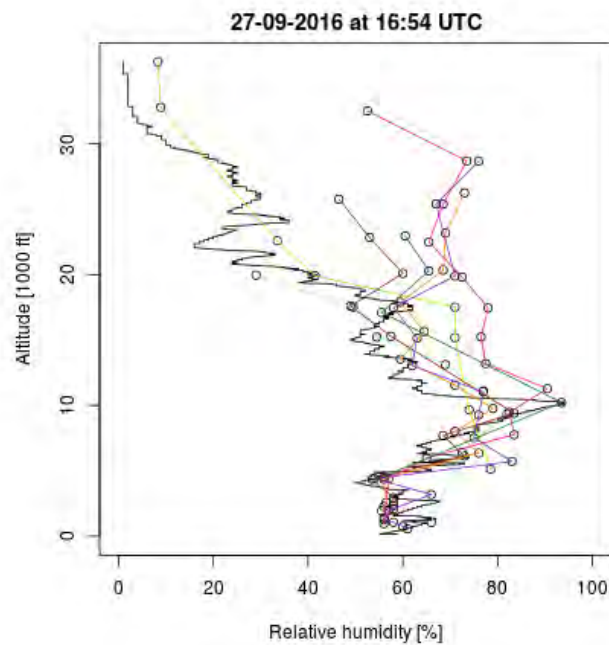

Figure 15: Relative humidity as measured by the radiosonde (black) and the TAMDAR (coloured) on 27 September 2016.

7.2 Case 2 - 29 September 2016
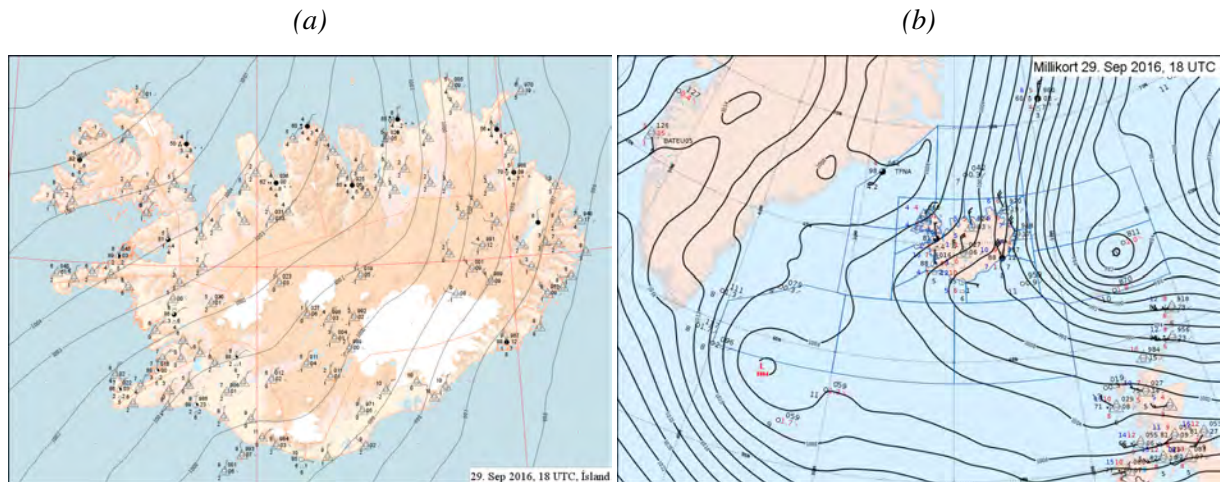
The weather situation

Figure 16: Synoptic weather charts for (a) Iceland and (b) the northern North Atlantic valid at 18 UTC on 29 September 2016.

On 29 September, a deepening low pressure system moved southwards along the east coast of Iceland. At noon, when it was closest to the coast, its center was about 200 to 300 nm off the east coast of Iceland and in the afternoon, it moved further to the south-east passing just north of the Faroe Islands in the evening. This low pressure system affected the weather in Iceland. A weak occluded front passed over Iceland in the afternoon and northerly winds prevailed. Under such conditions, the skies over the southern part of Iceland tend to be mostly clear, as much of the moisture in the cold air precipitates over North Iceland and the Icelandic highlands, resulting in relatively dry air reaching the southern part. This was indeed the case in Keflavík. Between 17 and 21 UTC that day, Keflavík METARs reported northerly winds at 14 to 17 knots, dispersed clouds at around 2000 ft and excellent visibility. Figure 16 shows synoptic charts for Iceland and the northern North Atlantic and Figure 17 shows forecast winds aloft over Iceland. All charts are valid at 18 UTC.
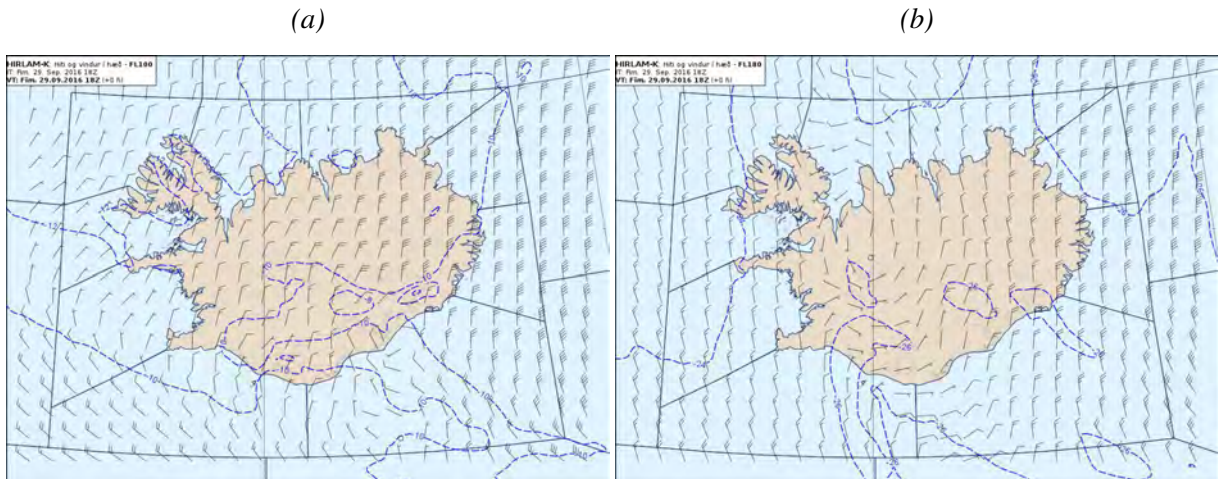
Figure 17: Winds aloft observed over Iceland according to the NWP model HIRLAM at the (a) 700 hPa and (b) 500 hPa pressure levels, valid at 18 UTC on 29 September 2016.

The measurements

A radiosonde was launched from Keflavík by the IMO at 17:01 UTC. Four flights with a total of 32 TAMDAR measurements, registered between 16:57 and 17:53, departed the airport within the time frame of the sonde. Table 6 gives an overview of these. Figure 18 shows the tracks of the TAMDAR flights along with the trajectory of the radiosonde. All of the TAMDAR measurements are logged west of the airport. Three of the flights follow very similar tracks while one of them, FIR (in brown), departs on a more northerly track than the others.

Table 6: An overview of TAMDAR measurements belonging to the radiosonde launched at 17:01 on 29 September. Measurements are broken down by airplane with the times of the first and last measurement of each plane, the number of measurements of each plane and an indication of whether the planes were departing or arriving at the airport.

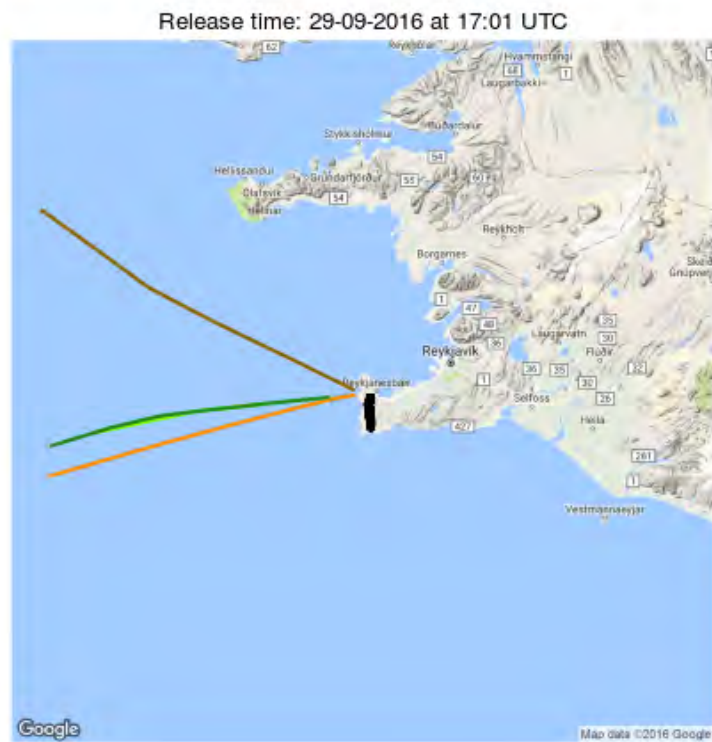| Aircraft	First log	Last log	Number of logs	DEP/ARR
FIU	16:57	17:10	12	DEP
FIR	17:09	17:24	11	DEP
FIJ	17:41	17:53	6	DEP
FIC	17:42	17:49	3	DEP

Figure 18: The tracks of TAMDAR flights (coloured) registered within the airspace shown and in the time frame of the radiosonde launched at 17:01 UTC on 29 September 2016, along with the trajectory of the radiosonde (black).

Figure 19 shows the temperature profile of the radiosonde along with all of the TAMDAR measurements associated with it. All of the measurements are in good agreement. The only TAMDAR measurement that markedly, yet only slightly, differs from the radiosonde's temperature profile is the measurement that is highest and furthest apart from the radiosonde in space, at an altitude of more than 25 thousand feet.
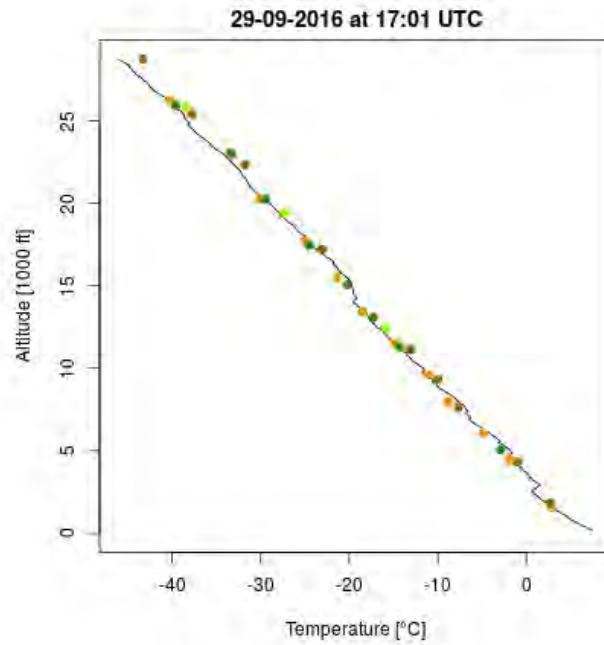

Figure 19: Temperature profile of the radiosonde along with TAMDAR temperature logs from 29 September 2016. The colours of the TAMDAR points correspond to the aircraft as shown in Figure 10.

The wind measurements of the radiosonde and the TAMDAR are compared in Figure 20. Below 10 thousand feet, many of the TAMDAR measurements are on or very close to the radiosonde profile. Above 10 thousand feet, there are larger discrepancies between the radiosonde and the TAMDAR. Note that FIR (in brown), that flies a different track to the other aircraft, measures much higher wind speeds than the other three above 10 thousand feet. FIC, FIU and FIJ, which all follow a very similar track, are quite consistent internally, however they also deviate considerably from the radiosonde's profile, especially between 15 and 20 thousand feet. Since those aircraft that follow a similar track are relatively consistent with each other, while the one that follows a different track is not, it is plausible that the measurements do to some degree represent a real spatial difference in wind speed. The greatest discrepancies between radiosonde and TAMDAR measurements amount to about 10 kts between 15 and 20 thousand feet. This difference is in accordance with the observed winds aloft in Figure 17b.

According to the radiosonde measurements, wind speed varies quite rapidly with height below twenty thousand feet. Note that, despite METAR reports of 14 to 17 kts on the ground in the afternoon and evening, the radiosonde repeatedly measures wind speeds below 10 kts up to a

height of about 18 thousand feet. Figure 20b shows measured wind direction. As before, measurements of 10 kts or less have been removed. Considering the rather calm conditions and high vertical variability, the overall consistency of the wind measurements is not bad.

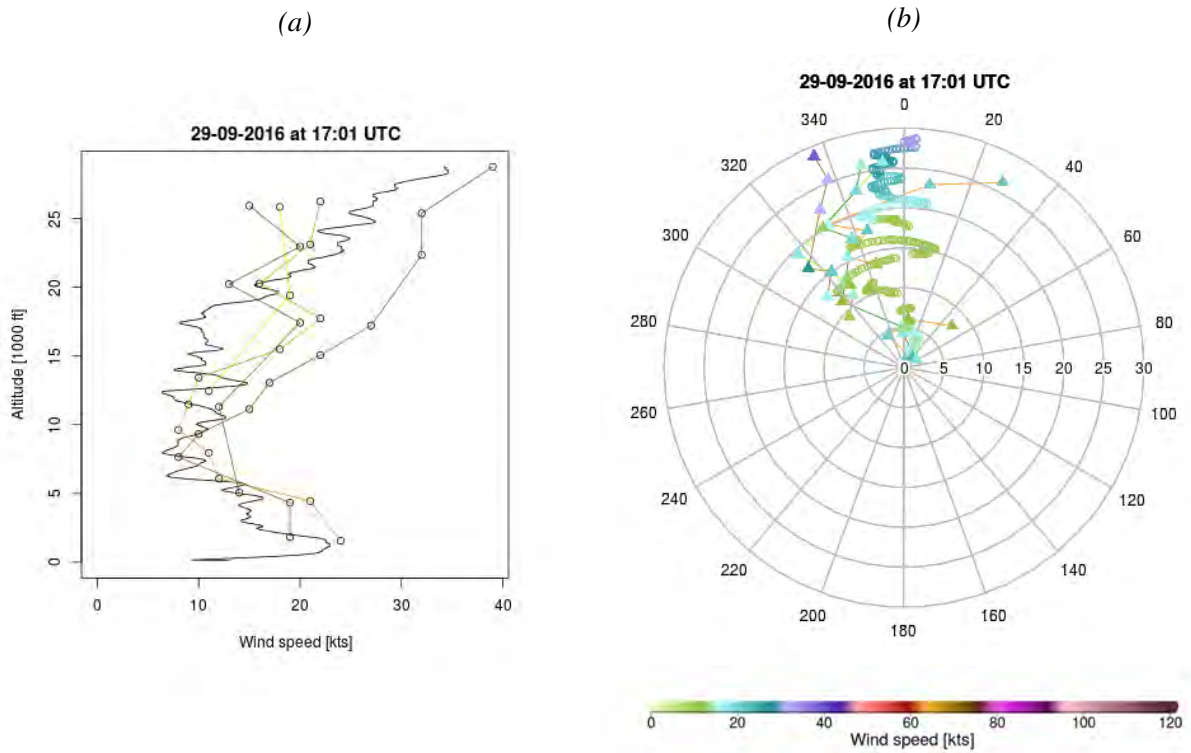*(a)*   *(b)*

Figure 20: (a) Wind speed profile of radiosonde (black) and TAMDAR (coloured) and (b) wind direction profile of radiosonde (circles) and TAMDAR (triangles and lines) on 29 September 2016. In (b), the radial axis represents altitude in thousands of feet while the angular axis represents wind direction in degrees. The colour scale applies to the wind speed shown by the triangles and the circles. Wind measurements of less than 10 kts have been removed. In both (a) and (b), the colour of the lines connecting TAMDAR measurements are in accordance with Figure 10.

Figure 21 shows a comparison of measured relative humidity values of the radiosonde and the TAMDAR. Almost all of the TAMDAR measurements yield a higher value for relative humidity than the radiosonde and between 14 and 20 thousand feet, many TAMDAR measurements indicate saturation while the radiosonde reports less than 90% relative humidity. The discrepancy between the TAMDAR and the radiosonde is markedly larger above 15 thousand feet than below this altitude. The TAMDAR measurements are relatively consistent with each other and despite some differences, their profiles all resemble each other.
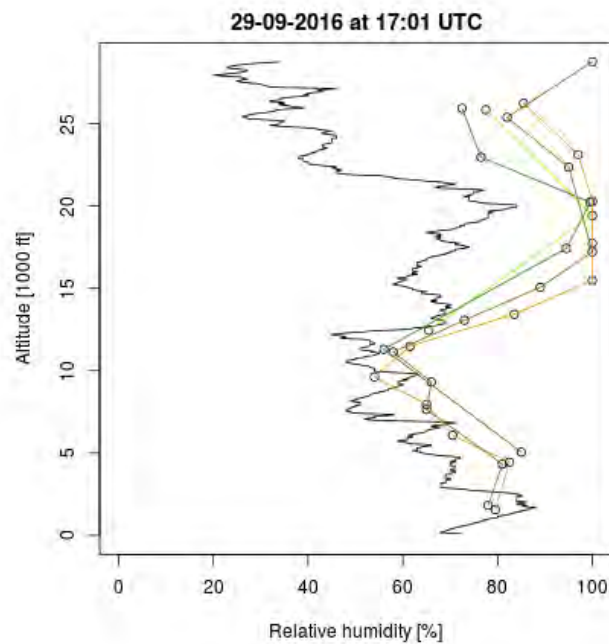

Figure 21: Relative humidity as measured by the radiosonde (black) and the TAMDAR (coloured) on 29 September 2016.

Figure 22 shows the relative humidity distribution according to the NWP model *Harmonie* on an east-west vertically cross sectional profile across Iceland. It predicts large differences in relative humidity along this profile around the 500 hPa pressure level, which corresponds to approximately 18 thousand feet. It is not unlikely that this high spatial contrast in relative humidity this afternoon in the vicinity of Keflavík would to some degree explain the difference in relative humidity measured by the radiosonde and the TAMDAR.
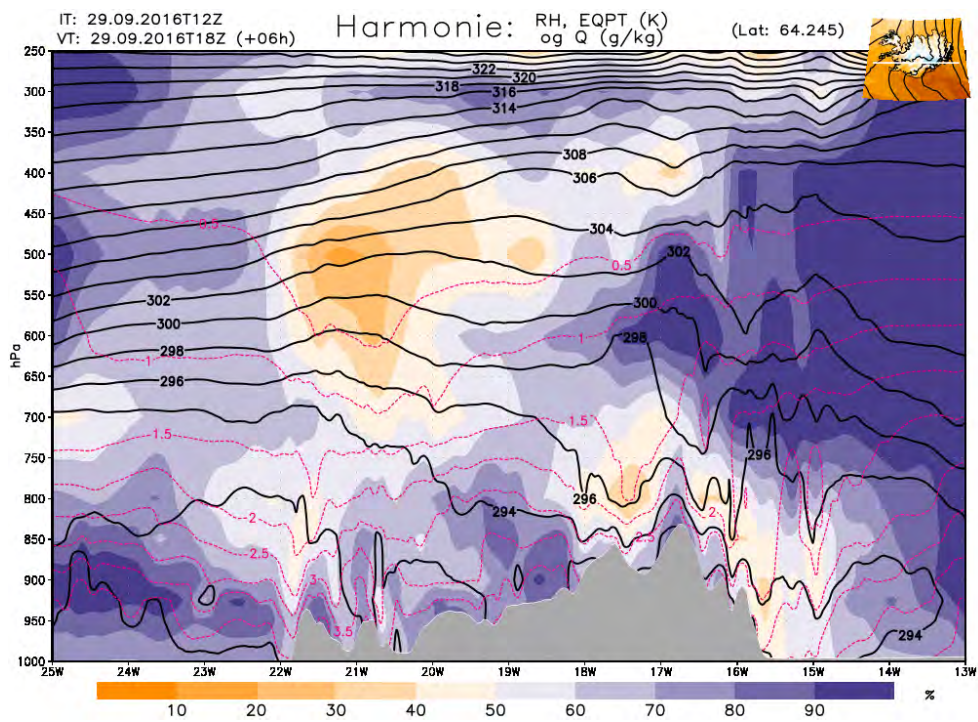
Figure 22: Forecast relative humidity over Iceland on a cross section along the 64.245°N parallel of latitude valid on 29 September 2016 at 18 UTC according to the NWP model Harmonie.

7.3   Case 3 - 1 October 2016
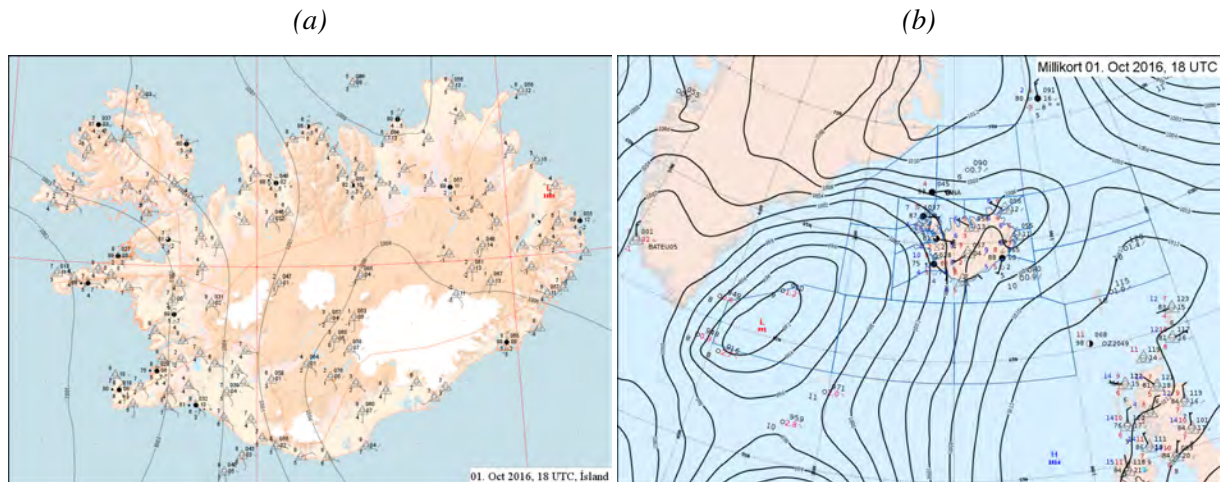
The weather situation

Figure 23: Synoptic weather charts for (a) Iceland and (b) the northern North Atlantic valid at 18 UTC on 1 October 2016.

On 1 October, an extensive low pressure system prevailed south-west of Iceland, with its center about 300 nm east of Cape Farewell, Greenland. The cyclone brought relatively moist and warm marine air over Iceland from lower latitudes. In the afternoon, as the low slowly deepened and its area of influence expanded to the north-east, the associated relatively weak warm front crossed the Reykjanes peninsula before continuing further inland. Synoptic charts of Iceland and the northern North Atlantic are shown in Figure 23 and the position of the front is shown in Figure 24. Both charts are valid at 18 UTC and at that time, the Keflavík METAR reported south-easterly 14 knots, three cloud layers of different coverage and rain.

Figure 25 shows two forecast charts for winds aloft. According to them, the wind over Keflavík strengthens and veers to a more westerly direction between the 500 and 300 hPa pressure levels, which correspond to approximately 18 and 30 thousand feet respectively. Note that the latter chart predicts markedly stronger winds to the west of Reykjanes than over the rest of the country and its coasts.

Figure 24: A synoptic weather chart showing fronts over the North Atlantic valid at 18 UTC on 1 October 2016.

(a)   (b)

Figure 25: Winds aloft observed over Iceland according to the NWP model HIRLAM at the (a) 500 hPa and (b) 300 hPa pressure levels, valid at 18 UTC on 1 October 2016.

33

The measurements

At 16:54 UTC on 1 October, the NAWDEX campaign launched a radiosonde from Keflavík. As mentioned in Section 7.3, a warm front passed over Keflavík around that time. Five TAMDAR carrying aircraft departed the airport and registered a total of 36 measurements between 16:23 and 17:59 UTC. See Table 7 for an overview of those.

Table 7: An overview of TAMDAR measurements belonging to the radiosonde launched at 16:54 on 1 October. Measurements are broken down by airplane with the times of the first and last measurement of each plane, the number of measurements of each plane and an indication of whether the planes were departing or arriving at the airport.

Aircraft	First log	Last log	Number of logs	DEP/ARR
ISD	16:23	16:34	8	DEP
LLX	17:32	17:45	5	DEP
FIU	17:34	17:46	8	DEP
FIP	17:43	17:59	10	DEP
FIJ	17:48	17:55	5	DEP

The tracks of the TAMDAR flights along with the radiosonde's trajectory are shown in Figure 26 below. As can be seen in the figure, four of the five flights follow very similar tracks west of the airport while one of them, ISD (light blue), departs the airport to the south-east.
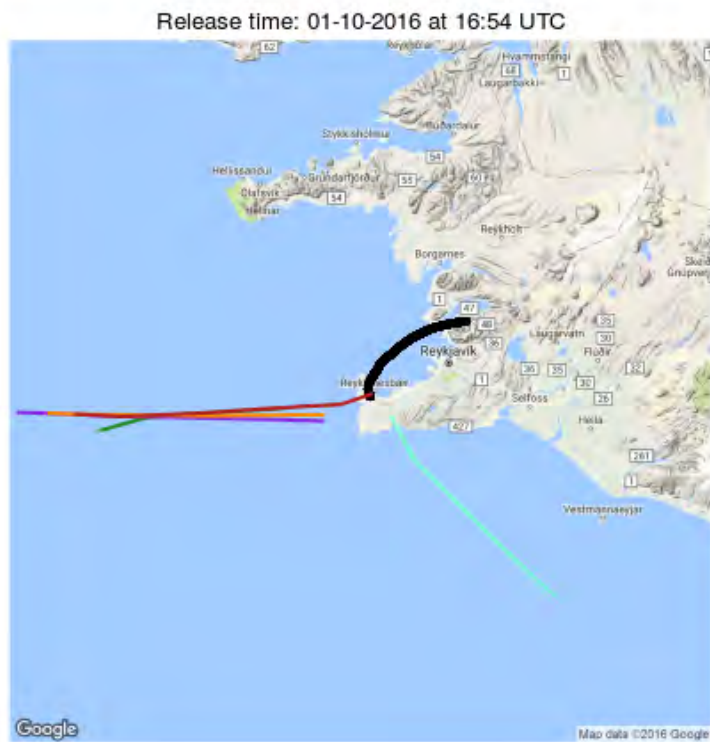
Figure 26: The tracks of TAMDAR flights (coloured) registered within the airspace shown and in the time frame of the radiosonde launched at 16:54 UTC on 1 October 2016, along with the trajectory of the radiosonde (black).

Figure 27 displays the radiosonde's temperature profile along with the TAMDAR temperature measurements. Most of the TAMDAR measurements fall on the radiosonde's temperature profile, but not all of them. The most notable exception is observed between 6 and 11 thousand feet, where three temperature measurements registered by FIP (dark red) are several degrees lower than the radiosonde and the other TAMDAR measurements. It is somewhat surprising that FIP registers such markedly lower temperatures than its colleague, FIU (yellow), which departed the airport along almost exactly the same track only about ten minutes earlier. As mentioned in Section 7.3, a warm front passed over Keflavík in the time frame of these measurements. According to the Norwegian cyclone model and common frontal theory, cold air precedes warm air upon the passage of a warm front. However, the measurements of FIP and ISD indicate that the opposite happened this afternoon. ISD, which departs along a very different track than the other flights, is in good agreement with the radiosonde as well as the TAMDAR measurements of the other flights. It is not unlikely that the low temperature values measured by FIP around 10 thousand feet are erroneous.
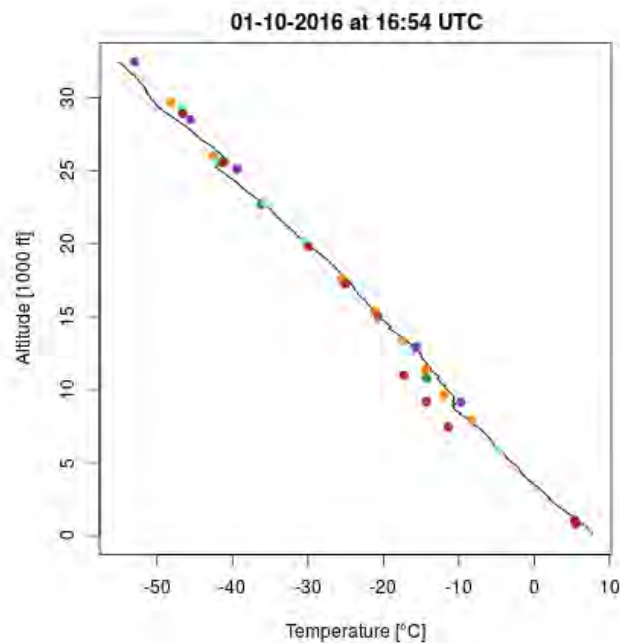

Figure 27: Temperature profile of the radiosonde along with TAMDAR temperature logs from 1 October 2016. The colours of the TAMDAR points correspond to the aircraft as shown in Figure 10.

Figure 28 displays wind speed and direction as measured by TAMDAR and the radiosonde. The TAMDAR is in good agreement with the radiosonde in this case, both in regards to wind speed and direction. Above 25 thousand feet, three of the aircraft that departed the airport to the west report a higher wind speed than the radiosonde and the aircraft that departed to the south-east. It is not unlikely that the great distance between the measurements at this altitude could explain this difference. In fact, according to the forecast chart in Figure 25b, wind speeds at about 30 thousand feet to the west of Reykjanes are markedly higher than winds at the same altitude off the south coast and over the west coast. Note also, that the charts in Figure 25 support the veering and strengthening of the wind with altitude which is measured by radiosonde and TAMDAR alike.
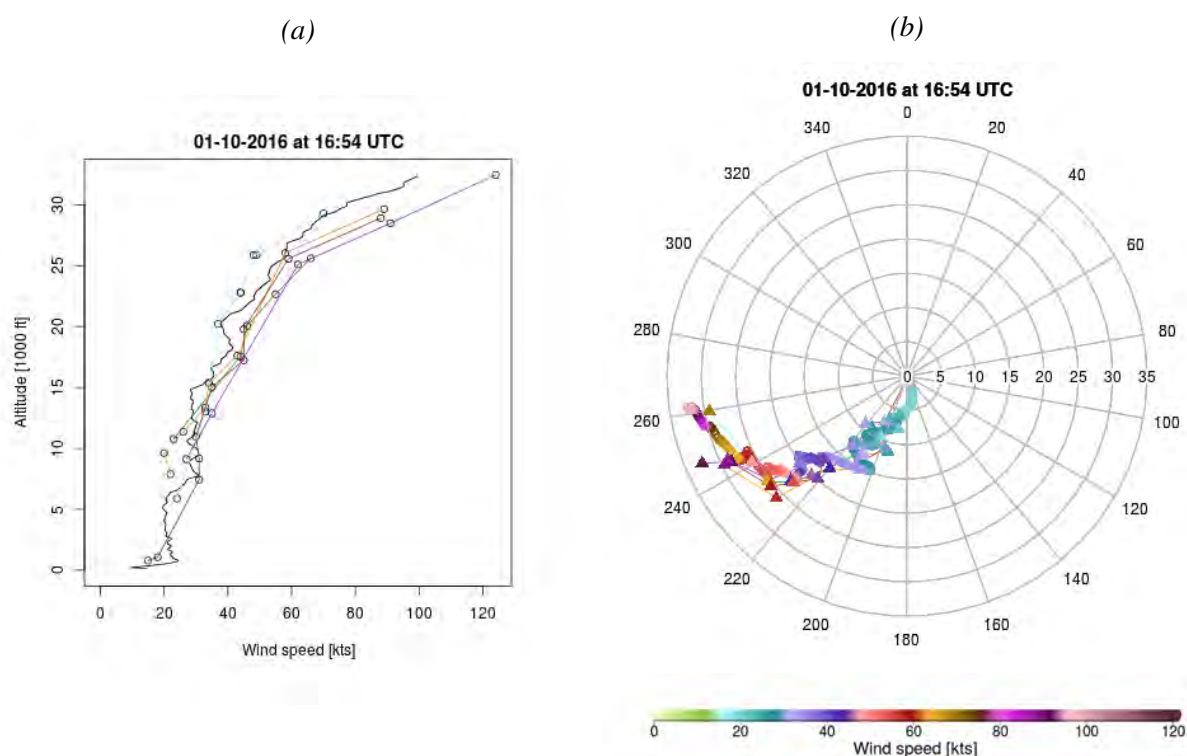

Figure 28: (a) Wind speed profile of radiosonde (black) and TAMDAR (coloured) and (b) wind direction profile of radiosonde (circles) and TAMDAR (triangles and lines) on 1 October 2016. In (b), the radial axis represents altitude in thousands of feet while the angular axis represents wind direction in degrees. The colour scale applies to the wind speed shown by the triangles and the circles. Wind measurements of less than 10 kts have been removed. In both (a) and (b), the colour of the lines connecting TAMDAR measurements are in accordance with Figure 10.

Relative humidity measurements are compared in Figure 29. As mentioned in Section 7.3, multiple cloud layers of different coverage were reported that afternoon and thus, the spatial variability of the relative humidity in the vicinity of Keflavík was likely such, that it cannot be assumed that all the aircraft and the sonde passed through the same cloud layers, as they followed different trajectories. Those aircraft that departed to the west are in relatively good agreement about the relative humidity. They did not detect the dry layer that the radiosonde passed through. However, ISD (light blue), which departed to the south-east, did detect this dry layer and its only

measurement at the altitude of the dry layer coincides with the radiosonde's profile. This is a further indication of significant spatial and/or temporal difference in relative humidity around Keflavík this afternoon. Many of the TAMDAR measurements report full saturation of the air at altitudes up to about 23 thousand feet.
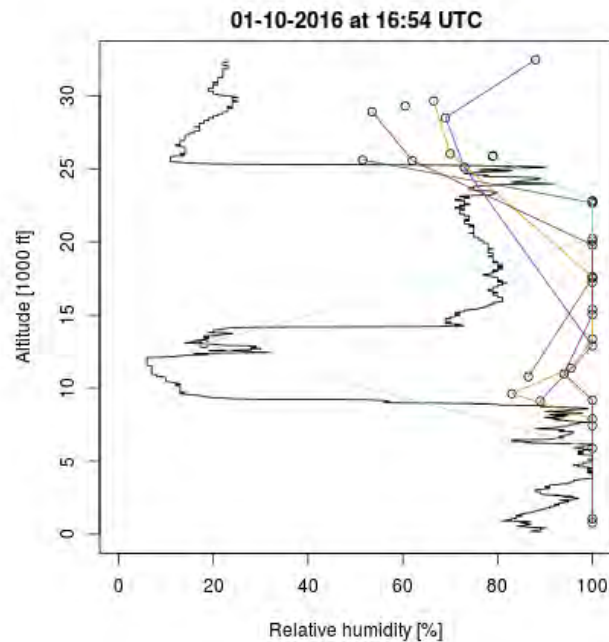

Figure 29: Relative humidity as measured by the radiosonde (black) and the TAMDAR (coloured) on 1 October 2016.

Figure 30 shows a relative humidity forecast from the NWP model *Harmonie* across an east-west profile over Iceland just north of Keflavík. Considering the fact that the radiosonde and ISD (light blue) departed on easterly tracks while the other aircraft departed to the west, this forecast does shed some light on the great difference in measured relative humidity. According to this forecast, to the west of Keflavík, relative humidity is close to 100% from the ground and up to 350 hPa (about 26 to 27 thousand feet). Below 24 thousand feet, this is in accordance with the profiles of the aircraft departing to the west. To the east of Keflavík, the NWP forecasts a layer of dry air at around 650 hPa (around 12 thousand feet). This matches the profile of the radiosonde. If this forecast cross section is characteristic for the situation in the airspace surrounding Reykjanes this afternoon, it would explain why ISD detected this dry layer while the other aircraft did not.
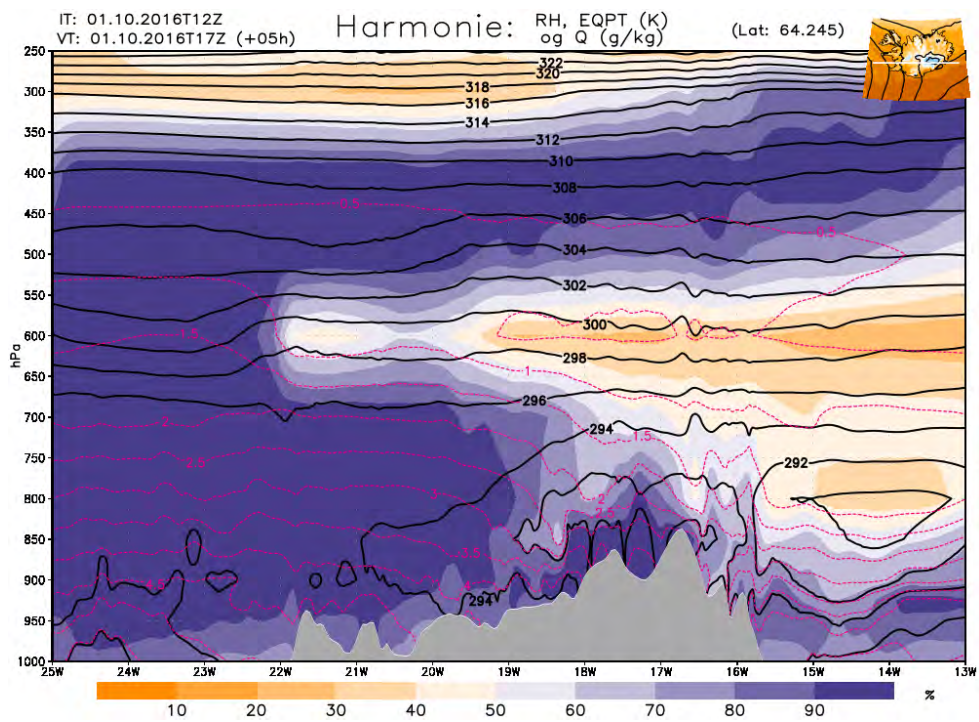
Figure 30: Forecast relative humidity over Iceland on a cross section along the 64.245°N parallel of latitude valid on 1 October 2016 at 17 UTC according to the NWP model Harmonie

7.4 Case 4 - 2 October 2016
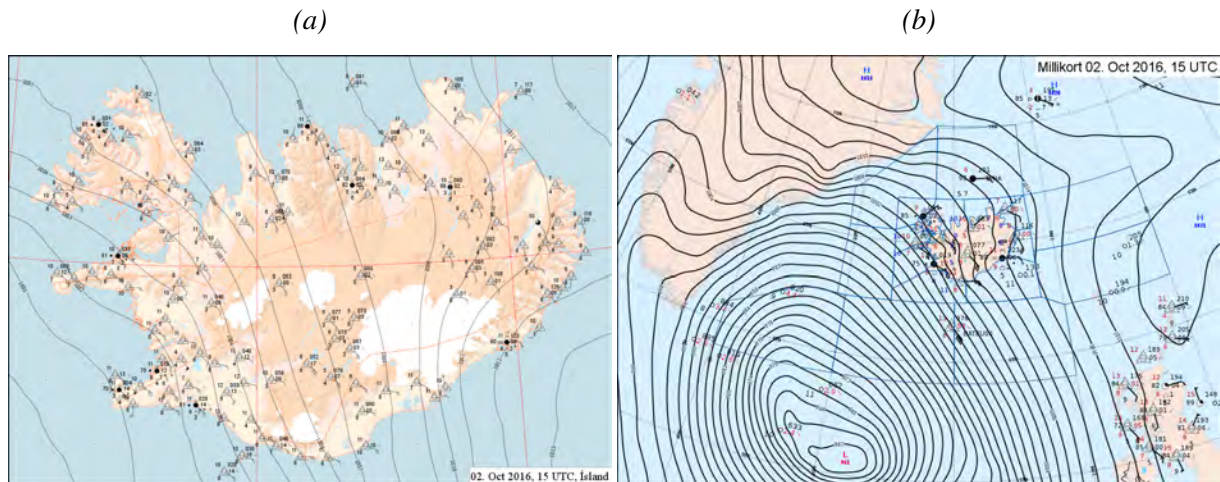
The weather situation

Figure 31: Synoptic weather charts for (a) Iceland and (b) the northern North Atlantic valid at 15 UTC on 2 October 2016.

On 2 October 2016, a rapidly deepening low pressure system approached Iceland from the south-west while a strong high pressure system prevailed close to Jan Mayen, north-east of Iceland. During the night, a warm front passed over south-west Iceland. Keflavík METARs reported showers, rain and a steady increase in wind speed from the early morning hours until the early afternoon. From the early afternoon until the early evening, Keflavík weather observations reported south-easterly winds at 30 to 33 knots with gusts exceeding 42 knots, which increased further towards the evening. Figure 31 show synoptic charts for Iceland and the North Atlantic at 15 UTC that day.

In the afternoon, a uniform south to south-easterly wind blew over Iceland at and above 10 thousand feet. Figure 32 shows weather charts for winds aloft at two different pressure levels, at approximately 10 and 18 thousand feet respectively as shown in Table 1. During the afternoon and until the early evening, the weather over Iceland did not change significantly.

The measurements

A radiosonde was released at 14:03 UTC on 2 October. Associated with it were 36 TAMDAR measurements. Table 8 gives an overview of the time and number of these.

Figure 33 shows the tracks of the TAMDAR flights and the trajectory of the radiosonde. The trajectories shown for ISY (magenta) and FIJ (dark green) do not reach the airport. This is due to their lack of measurements close to Keflavík. The reason for this lack is unknown. In this case, all measurements are made east or south-east of the airport.
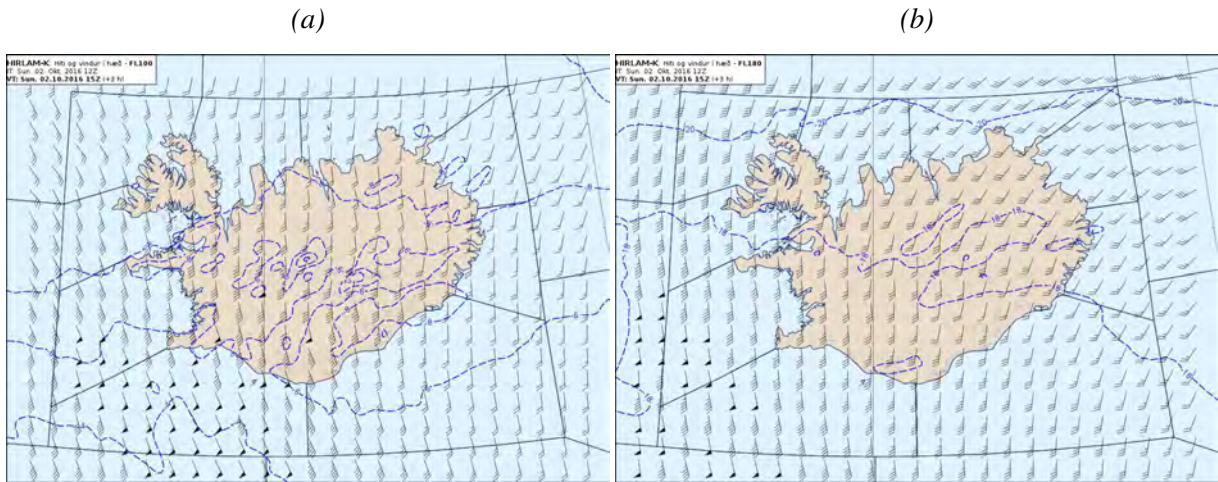
Figure 32: Winds aloft forecast over Iceland by the NWP model HIRLAM at the (a) 700 hPa and (b) 500 hPa pressure levels at 15 UTC on 2 October 2016.

Table 8: An overview of TAMDAR measurements belonging to the radiosonde launched at 14:03 on 2 October. Measurements are broken down by airplane with the times of the first and last measurement of each plane, the number of measurements of each plane and an indication of whether the planes were departing or arriving at the airport.

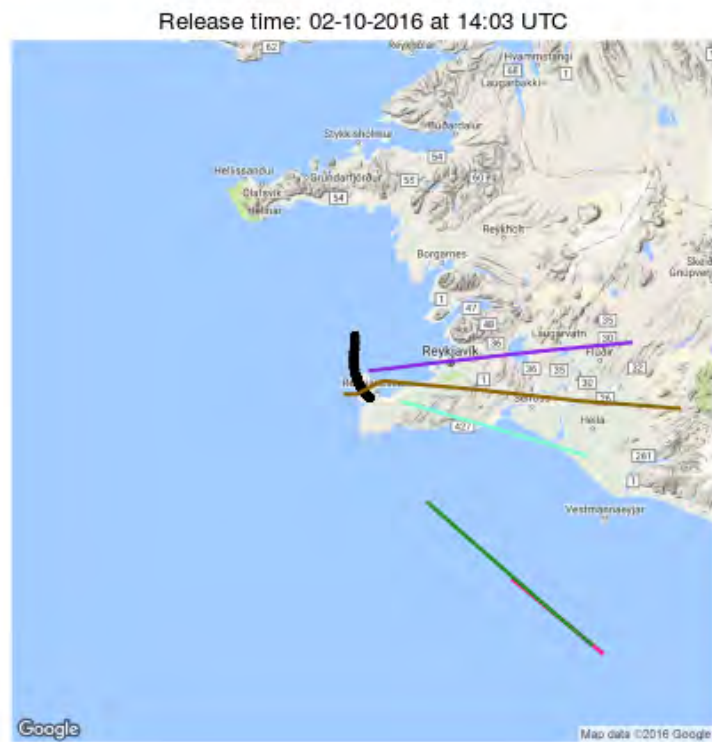| Aircraft	First log	Last log	Number of logs	DEP/ARR
ISD	13:25	13:34	5	DEP
ISY	14:44	14:48	4	ARR
FIR	15:03	15:24	15	ARR
FIJ	15:26	15:35	3	ARR
LLX	15:44	15:55	9	ARR

Figure 33: The tracks of TAMDAR flights (coloured) registered within the airspace shown and in the time frame of the radiosonde launched at 14:03 UTC on 2 October 2016, along with the trajectory of the radiosonde (black).

As shown in Figure 34, all TAMDAR temperature measurements seem to be in good accordance with the radiosonde. At about 14 thousand feet, the profile of the radiosonde indicates a temperature inversion and the TAMDAR captures this phenomenon. This high level of agreement, despite considerable distance between the radiosonde and the TAMDAR, indicates an excellent concordance between TAMDAR and radiosonde temperature measurements, even in windy conditions like those that prevailed over and around Keflavík this afternoon.
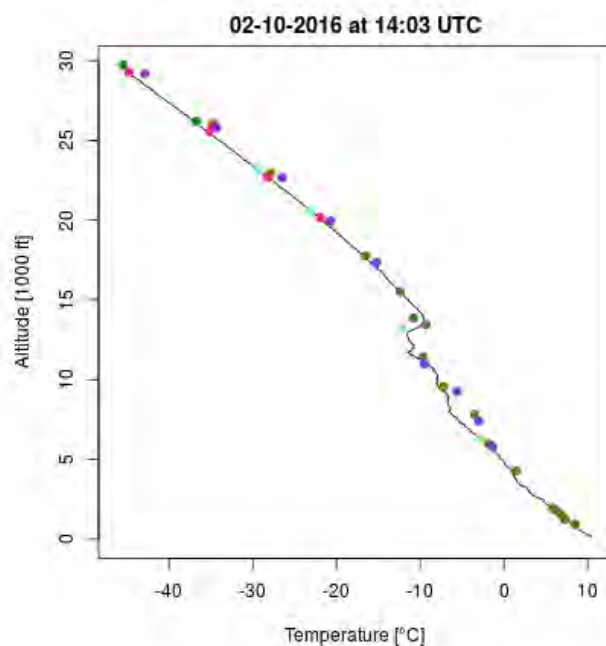

Figure 34: Temperature profile of the radiosonde along with TAMDAR temperature logs from 2 October 2016. The colours of the TAMDAR points correspond to the aircraft as shown in Figure 10.

During the ascent of the sonde, both wind direction and velocity remained relatively stable. Keflavík METARs reported a wind direction between 120 and 130 degrees from 14 until 16 UTC and wind speeds were reported between 30 and 32 kts, gusting at 42 to 45 kts during this time. Figure 35 shows measured wind speed of the radiosonde with TAMDAR measurements. The consistency of the registered wind speed measurements is generally good, but with some exceptions. The most noticeable exceptions are the two uppermost measurements made by FIJ (dark green) as well as three measurements made by FIR (brown) between 7 and 12 thousand feet which report much higher wind speeds than the sonde. Which, if any, of the measurements are faulty and which of them are closer to reality is difficult if not impossible to tell with the data available. The possibility that all of them represent a real scenario in which wind speed varied strongly in time and space cannot be eliminated. This might be the case, especially considering that 24 of the 36 TAMDAR measurements are made over or just north of the southern shore of the Reykjanes peninsula: in the wind direction observed in this case, strong, relatively undisturbed wind reaches the mountainous terrain of the peninsula. This sudden disturbance of the air is not unlikely to yield high temporal and spatial variability in wind in vicinity of the air-

port. In the majority of cases where the radiosonde and the TAMDAR strongly disagree on wind speed, the TAMDAR reports a much higher value than the radiosonde. This may indicate that the TAMDAR tends towards an overestimation of the wind speed compared to the radiosonde.

Below 15 thousand feet, wind direction measurements are in good agreement. Above 15 thousand feet, a greater deviation is observed, both generally between the radiosonde and TAMDAR as well as internally between different TAMDAR measurements. As mentioned in Section 7.1, the fact that measurement deviation increases with height is generally not surprising. However, as can be observed in Figure 35, the TAMDAR tends to report more easterly winds than the radiosonde above 15 thousand feet in this case. This might be a result of highly variable wind conditions around Keflavík as explained above.

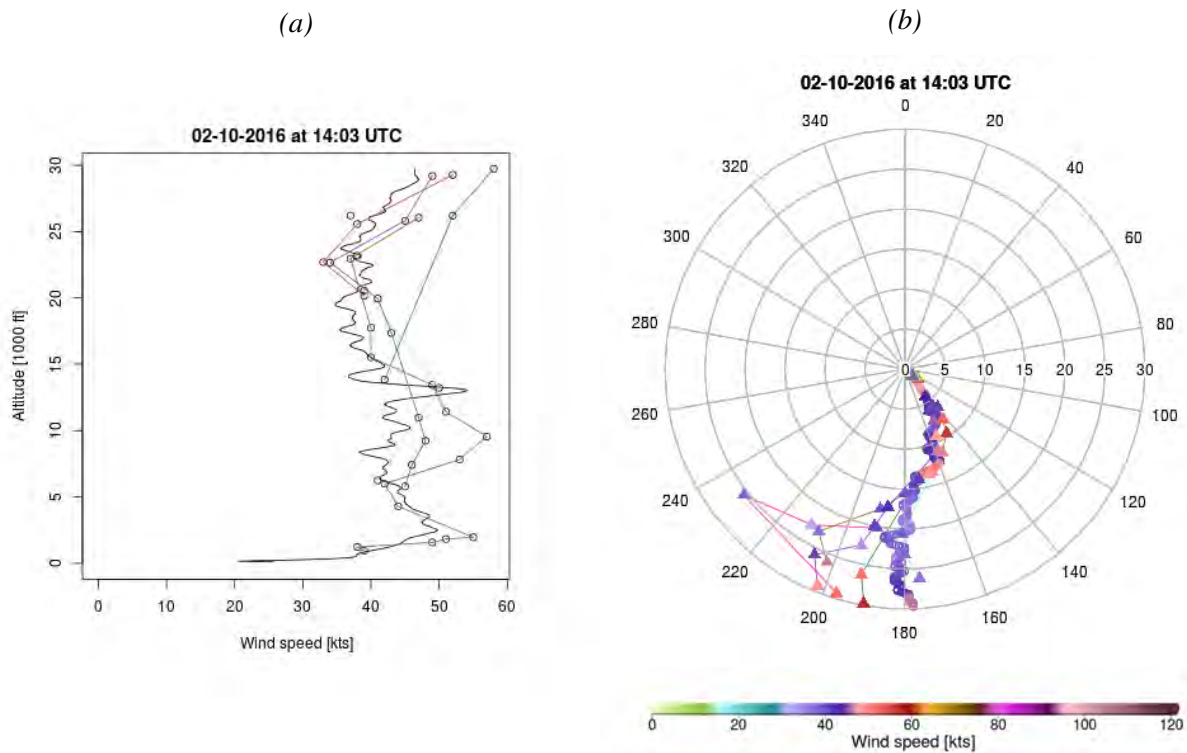*(a)*   *(b)*

Figure 35: (a) Wind speed profile of radiosonde (black) and TAMDAR (coloured) and (b) wind direction profile of radiosonde (circles) and TAMDAR (triangles and lines) on 2 October 2016. In (b), the radial axis represents altitude in thousands of feet while the angular axis represents wind direction in degrees. The colour scale applies to the wind speed shown by the triangles and the circles. Wind measurements of less than 10 kts have been removed. In both (a) and (b), the colour of the lines connecting TAMDAR measurements are in accordance with Figure 10.

44

Relative humidity measurements are compared in Figure 36. The TAMDAR seems to capture the overall trend of the sonde's relative humidity profile, especially below 15 thousand feet. Between 8 and 13 thousand feet, a layer of exceptionally dry air is detected by both the radiosonde and TAMDAR, although they seem to disagree slightly on its altitude. Note, however, that above 15 thousand feet, a majority of TAMDAR measurements report 100 % relative humidity. Even at 25 thousand feet, the TAMDAR measures full saturation of the air, which is in no accordance with the radiosonde measurements.
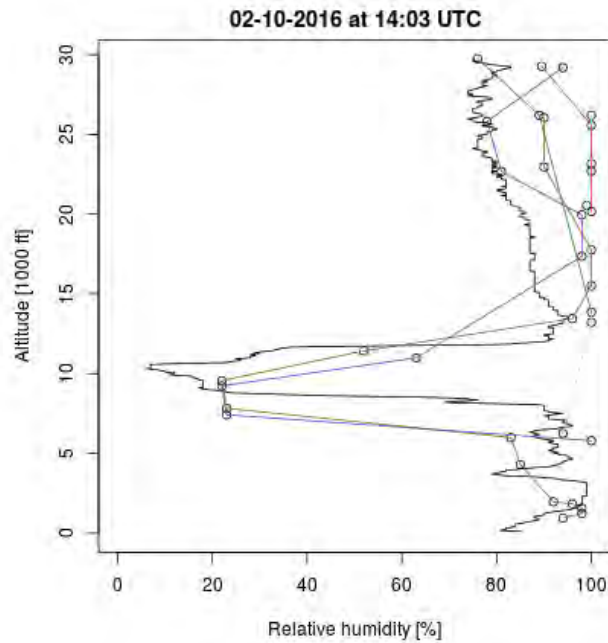

Figure 36: Relative humidity as measured by the radiosonde (black) and the TAMDAR (coloured) on 2 October 2016.

Figure 37 shows a NWP for relative humidity along a east-west profile across Iceland just north of Keflavík (the same profile as in the two previous chapters). A dry layer was predicted north of Reykjanes at around 700 hPa (about 10 thousand feet) this day. From the relative humidity measurements shown in Figure 36, it can be seen that the radiosonde and two of the flights, namely FIR (brown) and LLX (purple), detect the dry layer. The TAMDAR flights approach the airport from the east where, according to the forecast, the vertical extent of the dry layer is more than further west, where the radiosonde ascends. This is in accordance with the relative humidity profiles in Figure 36; the airplanes (FIR and LLX) detect the lower boundary of the dry air layer at a lower altitude than the radiosonde. The other three TAMDAR flights did not register any measurements at the altitude of the dry layer.

Figure 37: Forecast relative humidity over Iceland on a cross section along the 64.245°N parallel of latitude valid on 2 October 2016 at 15 UTC according to the NWP model Harmonie

7.5 Case 5 - 27 October 2016

The weather situation

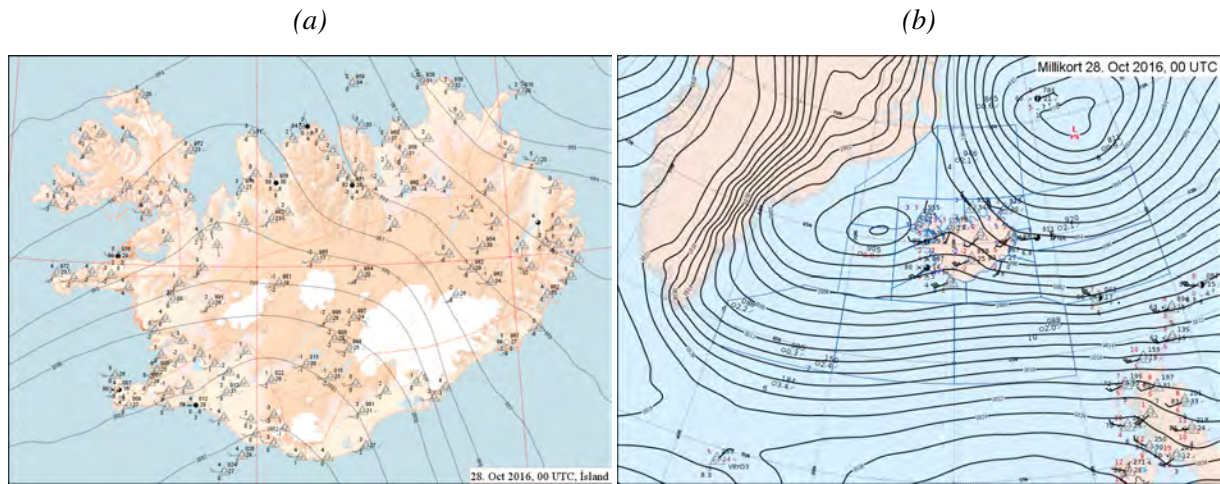*(a)*   *(b)*

Figure 38: Synoptic weather charts for (a) Iceland and (b) the northern North Atlantic valid at 00 UTC on 28 October 2016.

On 27 October 2016, two low pressure systems influenced the weather in Iceland. An extensive 976 hPa low prevailed south of Jan Mayen while a small scale, short-lived low formed just off the west coast of Iceland. In the afternoon, an occluded front passed over south-west Iceland. Throughout the day and the following night, periods of extensive convective build-up were observed in the vicinity of Keflavík and showers of rain and sleet with associated wind gusts passed over the airport. In the late evening and night, south-westerly winds were reported at 19 to 24 kts. At midnight, the Keflavík METAR reported gusts up to 32 kts, convective activity and showers in the vicinity. Figure 38 shows synoptic charts for Iceland and the North Atlantic and Figure 39 shows forecast winds aloft over Iceland that night. Both charts are valid at midnight.
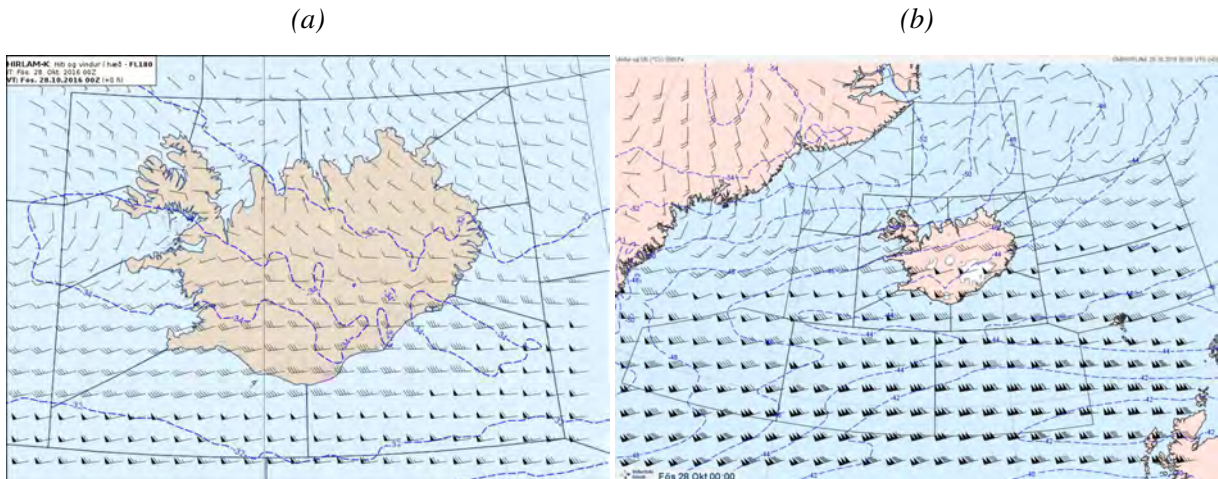
Figure 39: Winds aloft observed over Iceland according to the NWP model HIRLAM at the (a) 500 hPa and (b) 300 hPa pressure levels, valid at 00 UTC on 28 October 2016.

The measurements

A radiosonde was released by the IMO at 23:06 on 27 October. Between 23:15 and 23:48, two airplanes logged 37 TAMDAR measurements in the vicinity of Keflavík on tracks east and south-east of the airport. Table 9 gives an overview of the measurements and Figure 40 shows the tracks of the two flights along with the trajectory of the radiosonde.

Table 9: An overview of TAMDAR measurements belonging to the radiosonde launched at 23:06 on 29 October. Measurements are broken down by airplane with the times of the first and last measurement of each plane, the number of measurements of each plane and an indication of whether the planes were departing or arriving at the airport.

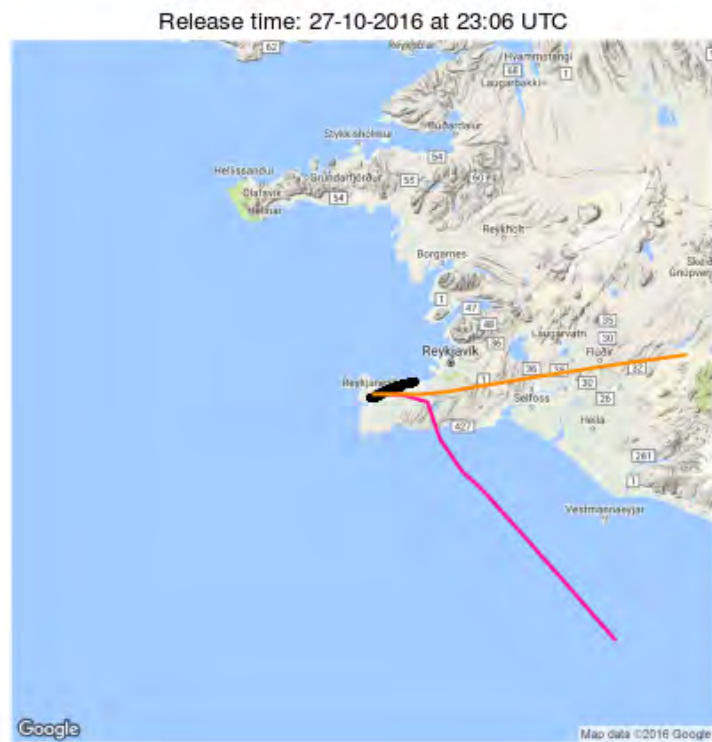| Aircraft	First log	Last log	Number of logs	DEP/ARR
ISY	23:15	23:34	17	ARR
FIU	23:28	23:48	20	ARR

Figure 40: The tracks of TAMDAR flights (coloured) registered within the airspace shown and in the time frame of the radiosonde launched at 23:06 UTC on 27 October 2016, along with the trajectory of the radiosonde (black).

Figure 41 shows a comparison of temperature as logged by the radiosonde and the TAMDAR. The figure shows how the temperature ceases to decrease with altitude around 25 thousand feet and then remains relatively steady. This marks the tropopause, as explained in Chapter 2. As usual, the temperature measurements of the radiosonde and the TAMDAR are in very good agreement.
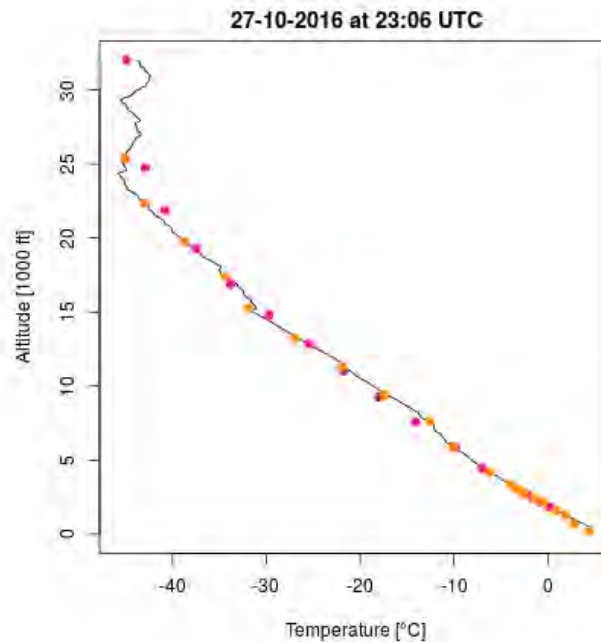

Figure 41: Temperature profile of the radiosonde along with TAMDAR temperature logs from 27 October 2016. The colours of the TAMDAR points correspond to the aircraft as shown in Figure 10.

A comparison of measured wind speed is shown in Figure 43a. In this case, the three profiles do not correspond very well because of the great difference in wind speed along their different tracks. Below 5 thousand feet, neither of the TAMDARs capture the profile of the radiosonde. Between 5 and 10 thousand feet, there is some similarity but above 10 thousand feet, the three profiles clearly diverge. FIU (yellow), which arrives from the east, measures a much lower wind speed than the radiosonde while ISY (magenta), which arrives from the south-east, measures much stronger winds. The difference in measured wind speed increases with altitude and at about 25 thousand feet, where the TAMDAR flights are furthest apart in space, they measure wind speeds that differ by more than 50 kts. In this case, the measurements were all made in the same 45 minutes and the time difference between measurements could hardly be further reduced with the methods used in this study. The spatial variability of the data is significant, but less so than in the other cases analyzed in this study. However, the position of the jet stream explains the difference. As shown in Figure 42, an area of very high wind speeds was observed just south of Iceland during the night. This area represents a part of the jet stream, which was briefly discussed in Chapter 3. As shown in Figure 40, ISY (magenta) passes through the jet on its approach to Keflavík whereas FIU (yellow) flies just north of the jet. The difference in recorded wind speeds along these two tracks is to be expected under the weather conditions present this evening.
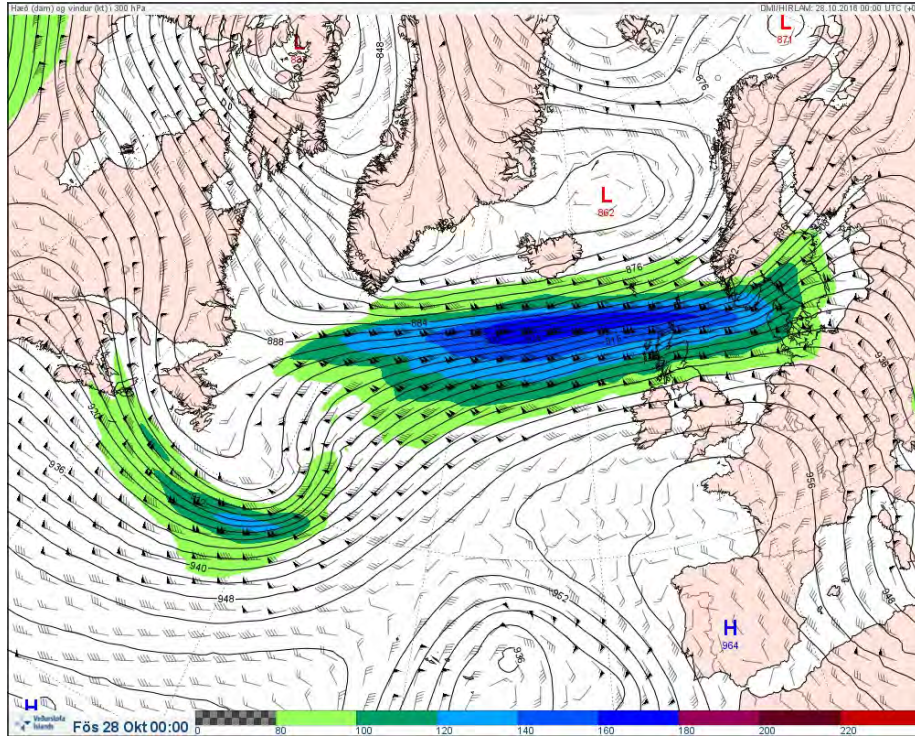
Figure 42: Observed winds aloft over the North Atlantic at the 300 hPa level on 28 October 2016 at 00 UTC according to the NWP model HIRLAM. Areas of wind speeds exceeding 80 knots are coloured in the figure. As shown in this figure, the jet stream passes just south of Iceland.

Figure 43b shows the measured wind direction. Below 15 thousand feet, both TAMDARs are in good agreement with the radiosonde. Above 15 thousand feet, ISY reports a slightly more northerly wind direction (about 270°) than FIU (closer to 250°). This is in accordance with the weather charts in Figures 39 and 42.
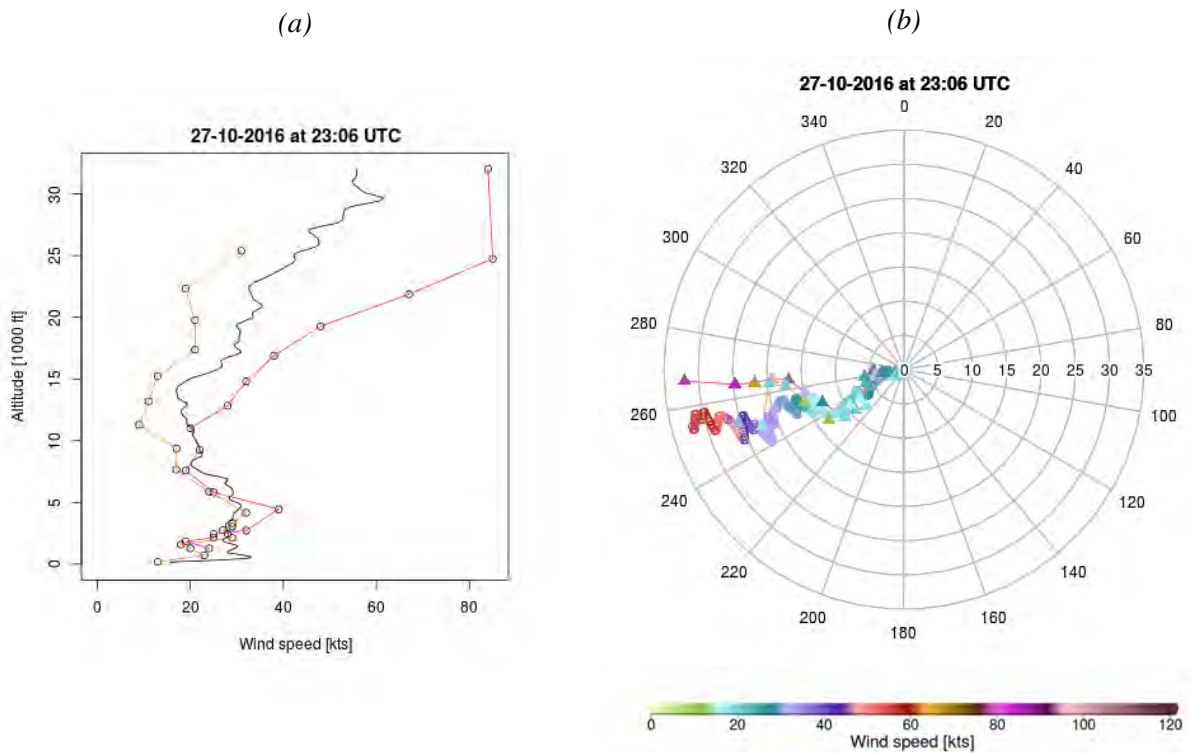
Figure 43: (a) Wind speed profile of radiosonde (black) and TAMDAR (coloured) and (b) wind direction profile of radiosonde (circles) and TAMDAR (triangles and lines) on 27 October 2016. In (b), the radial axis represents altitude in thousands of feet while the angular axis represents wind direction in degrees. The colour scale applies to the wind speed shown by the triangles and the circles. Wind measurements of less than 10 kts have been removed. In both (a) and (b), the colour of the lines connecting TAMDAR measurements are in accordance with Figure 10.

The profiles for measured relative humidity of TAMDAR and radiosonde are shown in Figure 44. Although all three profiles agree on the general trend of how relative humidity varies with altitude, some discrepancies are observed. Below 12 thousand feet, the majority of TAMDAR measurements report significantly higher relative humidity than the radiosonde. At and just below 5 thousand feet, several TAMDAR measurements report full saturation, and exceed the values registered by the radiosonde by more than 10 percent. Above 12 thousand feet, the air is dry and the concordance of the radiosonde and the TAMDAR is better than at lower altitudes. Overall, the TAMDAR captures the general trend of the radiosonde.
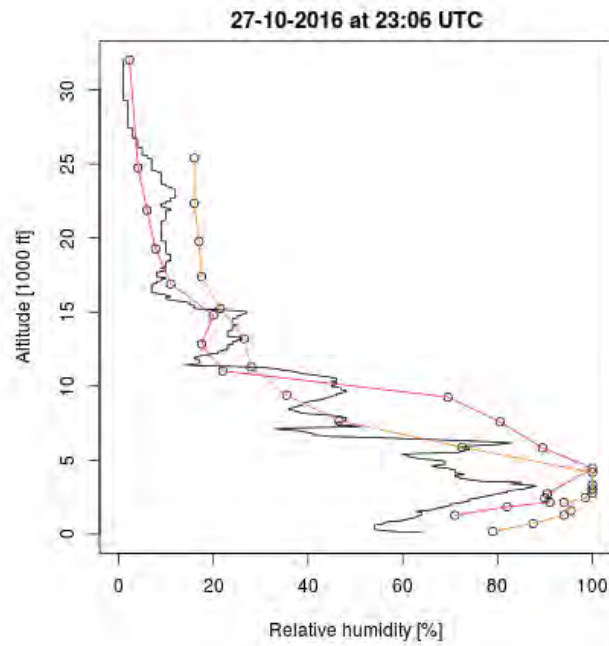

Figure 44: Relative humidity as measured by the radiosonde (black) and the TAMDAR (coloured) on 27 October 2016.

7.6   Spatial and temporal variations in the data

As mentioned at the beginning of and throughout this chapter, the time and distance that separate different measurements that have been made at the same altitude have a significant impact on the comparison analysis. This can make it difficult to draw conclusions regarding the quality and the actual consistency of the two measuring methods. In the following discussion, TAMDAR measurements from the above cases are compared to the measurement of their corresponding radiosonde that is closest to them in altitude. The difference between the TAMDAR value and the corresponding radiosonde value is plotted against the time and distance between the two measurements.

Figure 45 shows the distance and time between TAMDAR and radiosonde temperature measurements that correspond in the way described above. There is marked correlation between the temperature measurement discrepancies and the time and distance between them, as can be observed in the figure. Note, however, how modest these discrepancies are. The vast majority of the corresponding measurements fall within 2 degrees of each other. Three measuring points jump out for an unusually large discrepancy. These three points correspond to measurements made by FIP (dark red in Figure 27) on 1 October between 6 and 10 thousand feet. As discussed in Section 7.3, these three measurements were registered only about ten minutes after another airplane (FIU in yellow) departed Keflavík and registered a significantly higher temperature which was in accordance with the radiosonde as well as other measurements. The reason for these three unusually large discrepancies is not known, but it is not unlikely that the three outliers registered by FIP represent erroneous measurements.
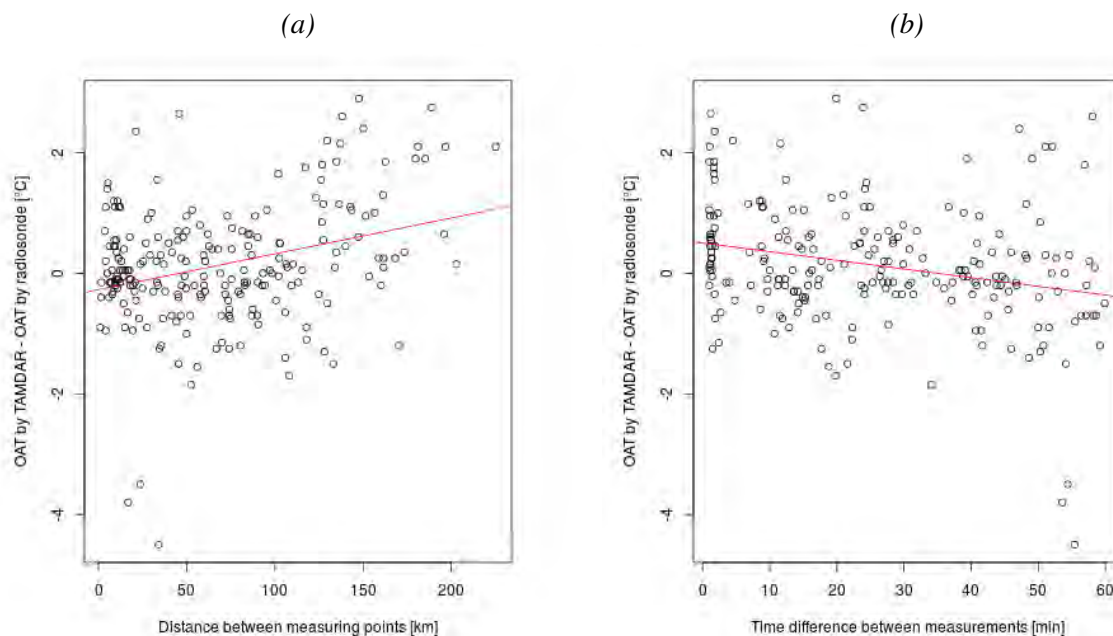

Figure 45: Difference between outside air temperature (OAT) measured by TAMDAR and radiosonde plotted against (a) distance and (b) time between measurements. A linear regression is shown in red. The calculated correlation is (a) 0.31 and (b) -0.26. In both cases, the p-value is less than 0.001

.

Figure 46 shows the distance and time between corresponding TAMDAR and radiosonde wind speed measurements. Here, the correlation is less marked than for the temperature measurements. This is especially true for the time difference, where the correlation is not significant. In the cases analyzed in this study, it is more common for the TAMDAR to measure a higher wind speed than the radiosonde than vice versa and in a few extreme cases, the TAMDAR values exceed the radiosonde values by more than 20, and beyond 40 kts. Note that the spread of discrepancy values increases with an increase in distance between measurements. However, the two most noticeable outliers are neither extremely far apart in space nor in time. They belong to two measurements which were registered by ISY (magenta in Figure 41) on 27 October between 20 and 25 thousand feet. In this case, ISY departs to the east while the radiosonde does not move very far from Keflavík. The radiosonde measures wind speeds around 5 kts at this altitude while ISY registers wind speeds of about 10 and 20 knots respectively. The reason for this disagreement is unknown.
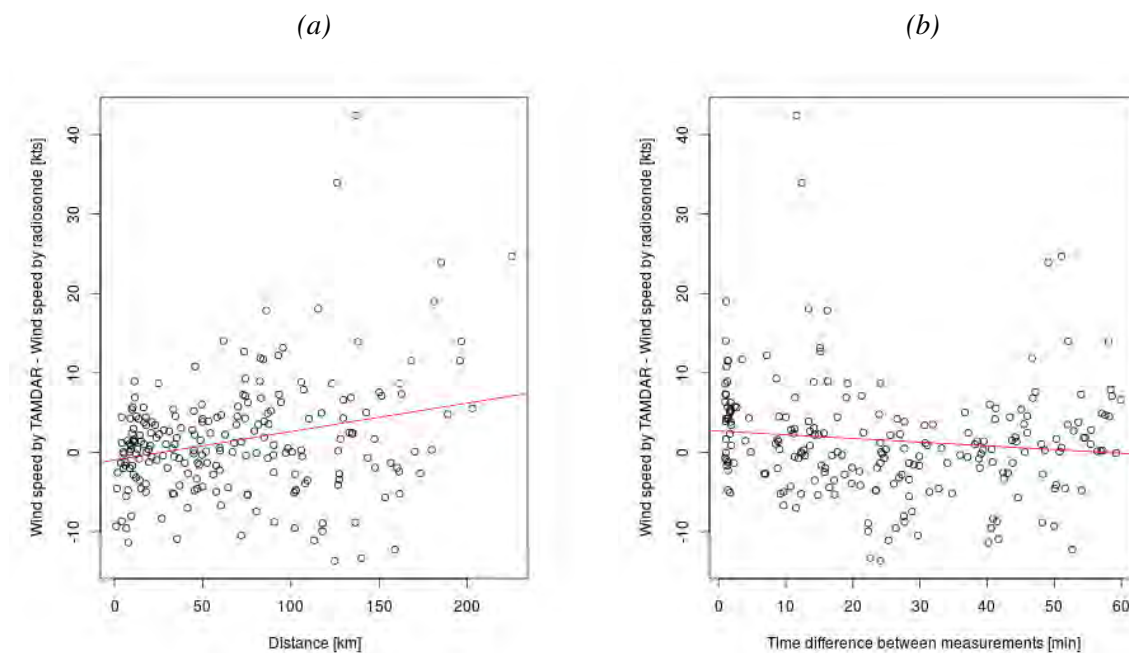

(a) *(b)*

Figure 46: Difference between wind speed measured by TAMDAR and radiosonde plotted against (a) distance and (b) time between measurements. A linear regression is shown in red. The calculated correlation and p-value are (a) 0.27 and less than 0.001 respectively (b) not significant and 0.08 respectively.

In Figure 47 are the differences in corresponding relative humidity measurements plotted against the spatial and temporal differences between them. Note the relatively large range of relative humidity discrepancies, especially in cases where the TAMDAR measures higher relative humidity than the radiosonde. This indicates that the spatial and temporal variability in relative humidity was rather large in the cases analyzed in this study. It might be an indication that the TAMDAR does generally tend to measure higher relative humidity than the radiosonde. However, as the sample consists of only 221 points gathered on five days, this observed tendency might be a coincidence. It cannot be ruled out that the TAMDAR flights in these cases coincidentally passed through more moist air or clouds than the radiosondes.

The six largest discrepancies in measured relative humidity all correspond to the same case, namely 1 October. As mentioned before, a warm front passed over Keflavík during the afternoon. The six outliers were all logged between 9 and 14 thousand feet, where the radiosonde detected a dry layer, while the aircraft that departed to the west did not. See Figure 29 for reference. Each of these flights is represented by one or more of the outliers mentioned here. As has been discussed in Section 7.3, NWPs indicate that this afternoon, a real spatial variability in relative humidity was present and this variability would to some degree explain the large discrepancies observed here.
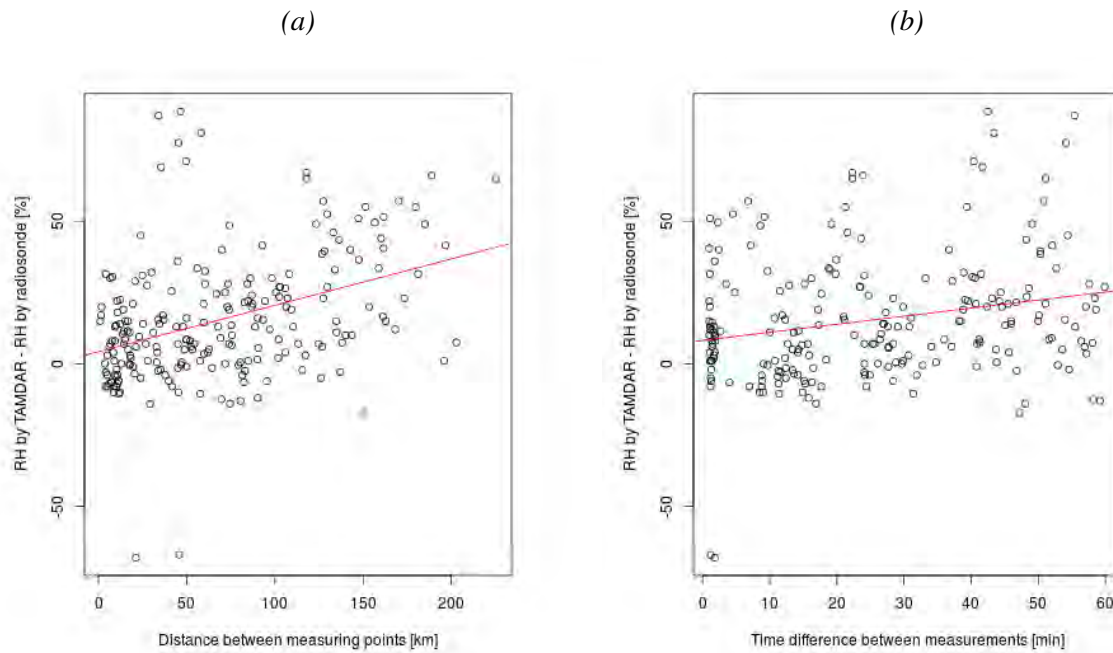

Figure 47: Difference between relative humidity (RH) measured by TAMDAR and radiosonde plotted against (a) distance and (b) time between measurements. A regression line is drawn through the set in red. The correlation given by the R cor.test function is (a) 0.39 and (b) 0.23. In both cases, the p-value is less than 0.001.

8 Conclusions

In this study, radiosonde and TAMDAR measurements were compared to each other as well as synoptic and NWP weather charts in five cases in an effort to assess the quality and correspondence of data gathered by radiosondes and TAMDAR. The aim of the study was to evaluate to what extent the use of TAMDAR measurements should be implemented in observing and forecasting aviation weather conditions in Icelandic airspace. Due to the nature of the data available, the constraints that were put on the distance between the data points compared were relatively weak. These constraints are described in detail in Chapter 6.

For the cases analyzed in this work, the following observations were made:

1. Temperature measurements of radiosondes and TAMDAR are generally in very good agreement. This applies also to measurements that are relatively far apart in time and space and suggests that in the cases analyzed in this study, spatial and temporal temperature variations were relatively small and that radiosondes and TAMDAR are generally highly consistent in their temperature measurements.

2. Wind speed measurements of radiosondes and TAMDAR are sometimes consistent with each other. It is often possible to explain discrepancies between radiosonde and TAMDAR with observed or forecast spatial wind variations. In all of the cases studied here, the wind speed profile of the TAMDAR resembles the wind speed profile of the radiosonde at some altitudes, even if it is sometimes offset from the profile of the radiosonde.

3. Below 20 thousand feet, wind direction data from radiosonde and TAMDAR are highly consistent. Above 20 thousand feet, the discrepancies between wind direction measured by radiosonde and TAMDAR can to some degree be explained by spatial variations in wind direction according to synoptic weather charts. Generally, the TAMDAR seems to give a good estimate of wind direction.

4. Relative humidity measurements of radiosonde and TAMDAR are often difficult to compare with the methods used in this study due to the relatively high spatial and temporal variability in relative humidity. However, in the cases analyzed here, the TAMDAR seems to capture variations in humidity with altitude. Discrepancies between radiosonde and TAMDAR measurements can to some degree be explained by a spatial variability in relative humidity according to NWPs. The resolution and accuracy with which the TAMDAR captures variations in relative humidity cannot be concluded from the data available.

5. In the cases analyzed in this study, discrepancies between TAMDAR and radiosonde measurements were more correlated with the distance than the time between them. This suggests that, given a higher abundance of data, putting tighter spatial constraints on the distance between data points to be compared would have yielded significantly stronger results.

The results of this study indicate that the use of atmospheric data gathered by TAMDAR to forecast and assess weather conditions in Icelandic airspace would prove a good supplement to the radiosonde data on which atmospheric profiling in Iceland is primarily based at present. The coverage and frequency of TAMDAR soundings is such, that incorporating them into the observation system of the IMO would provide a healthy addition to traditional observing methods, at a modest cost. As mentioned above, a higher abundance of data would likely yield stronger results, since this will allow for a reduction in the spatial variability of the data. However, it is recommended that the quality of TAMDAR data be further studied and continuously monitored, making use of larger datasets gathered over longer time periods than in this study. Until the the accuracy and resolution of TAMDAR has been further researched and monitored in this way, TAMDAR alone should not be solely relied upon for observations and forecasting.

9 References

Annex, I.C.A.O. (1998, July). 6 - Operation of Aircraft. ICAO Annex.

Annex, I.C.A.O. (2010, July). 5 - Units of Measurements to be Used in Air and Ground Operations. ICAO Annex.

Barry, R.G., & Chorley, R.J. (2010). *Atmosphere, Weather and Climate (9th ed.)* New York, NY: Routledge.

Batchelor J., & Lowe, M.V. (2006). *The Complete Encyclopedia of Flight 1848 - 1939 (2nd ed.)* Lisse: Rebo International.

Crocker, M.J. (1998). *Handbook of acoustics*. New York, NY: John Wiley & Sons.

Daniels, T. S. (2002). *Tropospheric airborne meteorological data reporting (TAMDAR) sensor development* (No. 2002-01-1523). SAE Technical Paper.

DuBois J.L., Multhauf R.P., Ziegler, C.A., & Smithsonian Institution (2002). *The Invention and Development of the Radiosonde: With a catalog of upper-atmosphere telemetering probes in the National Museum of American History, Smithsonian Institution* (Vol. 53). Washington D.C.: Smithsonian Institution Press.

Garðarsson, H. (1999). *Saga Veðurstofu Íslands*. Reykjavík: Mál og Mynd.

HMSO (1994). *Handbook of Aviation Meteorology (3rd ed.)*. London, UK: HMSO Publication Centre.

Jóhannsson, A.T. (2016). *Atmospheric Sounding by TAMDAR over Keflavík Airport, Iceland - Comparison with Traditional Atmospheric Sounding Methods, B.Sc. thesis*. Faculty of Earth Sciences, University of Iceland.

Mulally, D.J., & Anderson A. (2011, January). *Correction of Aircraft Flux Valve Based Heading for Two-Dimensional Winds Aloft Calculations Using Weather Model Comparisons*. 15th Symposium on Integrated Observing and Assimilation Systems for Atmosphere, Oceans and Land Surface (IOAS-AOLS), Seattle, WA.

Mulally, D.J., & Braid J.T. (2009, January). *The TMADAR sensor's relative humidity performance on ERJ-145 commercial aircraft*. 13th Symposium on Integrated Observing and Assimilation Systems for Atmosphere, Oceans and Land Surface (IOAS-AOLS), Phoenix, AZ.

National Research Council (2001). *Commercial Supersonic Technology: The Way Ahead*. Washington DC: The National Academies Press.

Newton, I. (1687). *Philosophiæ Naturalis Principia Mathematica*.

NOAA (nd.). *Layers of the Atmosphere*. Retrieved on 6 December 2016 from `http://www.srh.noaa.gov/srh/jetstream/atmos/layers.html`.

Oxford Aviation Academy (2011). *ATPL Ground Training Series: Principles of flight (6th ed.)* Shoreham, England: Transair Ltd.

Panasonic (2016). *Here's How Panasonic Is Redefining Weather Forecasting*. Retrieved on 6 December 2016 from `http://panasonic-betterlife.com/radical-change-weather-forecasting/`.

R Core Team (2016). R: A language and environment for statistical computing. R Foundation for Statistical Computing, Vienna, Austria. ISBN 3-900051-07-0, URL `http://www.R-project.org/`.

Schipper, J. & Zwatz-Meise, V. (2005). *Cyclogenesis according to the classical polar front theory*. Retrieved on 6 December 2016 from `http://www.eumetrain.org/data/2/2/cyclo.htm`.

Vaisala (2010). *User's Guide. Vaisala Radiosonde RS92-D*. Retrieved on 21 November 2016 from `http://www.vaisala.com/en/products/soundingsystemsandradiosondes/radiosondes/Pages/RS92.aspx`.

Vaisala (2010). *Vaisala Radiosonde RS92-D*. Retrieved on 12 November 2016 from `http://www.vaisala.com/VaisalaDocuments/BrochuresandDatasheets/RS92-D-Datasheet-B210763EN-B-LoRes.pdf`.

Vaisala (2016). *User Guide. Vaisala Radiosonde RS41-SG and RS41-SGP*. Retrieved on 21 November 2016 from `http://www.vaisala.com/en/products/soundingsystemsandradiosondes/radiosondes/Pages/RS41.aspx`.

Vaisala (2016). *Vaisala Radiosonde RS41-SG*. Retrieved on 12 November 2016 from `http://www.vaisala.com/VaisalaDocuments/BrochuresandDatasheets/WEA-MET-RS41-Datasheet-B211321EN.pdf`.

Wai-hung Leung (2010, December). *Geostrophic Wind*. Retrieved on 6 December 2016 from `http://www.weather.gov.hk/m/article_e.htm?title=ele_00010`.

Wallace, J.M., & Hobbs, P.V. (2006). *Atmospheric Science. An Introduction survey (2nd ed.)*. Oxford, UK: Elsevier Inc.

World Meteorological Organization (WMO) (2014). *Manual on Codes. International Codes. Volume I.1. Part A - Alphanumeric Codes. (2011 ed. updated in 2015)*. Retrieved on 14 November 2016 from `http://www.wmo.int/pages/prog/www/WMOCodes/WMO306_vI1/Publications/2014update/306_vol_I1_2014_en_track.pdf`.

World Meteorological Organization (WMO) (2016). *About The WMO AMDAR Observing System*. Retrieved on 3 December 2016 from `http://www.wmo.int/pages/prog/www/GOS/ABO/About_AMDAR.html`.

Conflict of Interests Declaration

The author of this thesis hereby declares that no conflict of interests exists regarding its publication.